



Effectiveness of Different Reinforcement Alternatives for Mitigating Liquefaction in Sands

Balaji Lakkimsetti¹ · Gali Madhavi Latha¹

Received: 8 March 2023 / Accepted: 8 June 2023 / Published online: 18 June 2023
© The Author(s), under exclusive licence to Springer Nature Switzerland AG 2023

Abstract

Liquefaction in sands is a natural hazard associated with an earthquake and remains a major concern for geotechnical engineers, as the shear strength of saturated loose sands reduces drastically with the development of positive pore pressures under dynamic loads resulting in the breakage of grain contacts. Traditional remedial measures to avoid liquefaction include densifying the ground, installing vertical drains to dissipate the pore pressures, and grouting with binders to impart cohesion. These techniques are not sustainable as they are quite expensive, energy, and resource intensive. This study examines the efficacy of various sustainable alternatives for mitigating the liquefaction hazard in sands, including the use of polymeric geotextiles, geofoam, coir fibers, and encased granular columns, and compares their performance. For this, a series of constant volume cyclic simple shear tests were performed on the sand in its natural condition and after modification with different techniques. Loading intensity is varied to simulate different seismic scenarios. Results are interpreted in terms of pore pressures, shear strains, energy dissipation, and modulus degradation, and the efficacy of these techniques for liquefaction mitigation is quantified and compared. Internal mechanisms responsible for the improvement in liquefaction resistance through different techniques were critically examined. It was found that the liquefaction resistance of sand increased using these techniques. However, the maximum benefit is found to be with the inclusion of geofoam, followed by encased granular columns, coir fibers, and geotextile. Findings from this study have direct relevance for capacity building against earthquakes through different sustainable methods.

Keywords UNSDG11: sustainable cities and communities · Liquefaction · Earthquakes · Sustainability · Geosynthetics · Cyclic simple shear test

Introduction

Earthquakes are the most dangerous, naturally occurring events that pose various hazards to human life and infrastructure [1]. Liquefaction of soils is one such natural hazard associated with earthquakes that have the potential to severely impact societal stability. Many times, civil and hydraulic engineering structures like retaining walls, earth-fill dams, and bridge abutments are usually backfilled with granular materials like sand. Liquefaction of sands is the primary reason for the failure of these structures under seismic

loadings, as the soil is in contact with the water in these structures due to several reasons like rainwater infiltration, seepage flow into the dams, and poor drainage conditions [2–4]. For example, the 2010 Darfield earthquake, 2011 Christchurch earthquake, 2015 Nepal earthquake, 2017 Chile earthquake, and 2018 Indonesia earthquake resulted in mass destruction and damage to the infrastructure due to large-scale soil liquefaction [5–7].

Liquefaction is often associated with a sudden loss of shear strength accompanied by rapid deformations. Lateral spreading, sand boiling, slope failures, and loss of bearing capacity are all consequences of extreme soil liquefaction events [2]. The pore pressure builds up in saturated sands under undrained conditions when subjected to dynamic loads due to their affinity toward contraction. This building up of excess pore pressure disturbs the load-carrying soil skeleton and converts it into a suspension with minimal residual strength by breaking the grain contacts resulting

✉ Balaji Lakkimsetti
lakkimsettib@iisc.ac.in

Gali Madhavi Latha
madhavi@iisc.ac.in

¹ Department of Civil Engineering, Indian Institute of Science
Bangalore, Bengaluru 560012, India

from the reduction of effective stresses that hold them [8, 9].

Studies on the liquefaction response of sands paced up after the severity of the destruction associated with this phenomenon was discovered during the 1964 Alaska and Niigata earthquakes [10]. Liquefaction phenomenon is studied both in laboratory element scale tests like cyclic triaxial, simple shear, and torsional shear tests and in model tests like shaking table and centrifuge tests [11–14]. The cyclic simple shear test was found to better represent the idealized seismic loading by allowing the continuous rotation of principal stresses during shearing when compared to other element tests [15–17]. The liquefaction potential of sand was found to be dependent on its relative density, degree of saturation, fines content, stress history, and particle morphology [18–22]. Conventional methods to modify the existing ground to improve its liquefaction resistance include densifying the ground using vibrocompaction, installing prefabricated vertical drains to enhance drainage conditions, and injecting cementitious binders to impart apparent cohesion between the grain contacts.

Vibrocompaction involves the usage of a compaction probe that transmits a tremendous amount of vibration energy generated by oscillating eccentric weights at a high frequency of up to 20 Hz to densify the cohesionless sands [23, 24]. The probe is lowered at a rate of 2.0 m/min until the required treatment depth is reached and withdrawn at a rate of 1.2 m/min. For treating a large area, compaction has to be done based on an optimally designed compaction grid spacing [25]. This method is highly energy intensive, involving the usage of large crawler cranes of 50-ton capacity carrying a 7 ton vibrator [26].

Providing prefabricated vertical drains (PVDs) expedites the dissipation of excess pore pressures by modifying the flow patterns [27, 28]. These are perforated hollow plastic tubes with diameters ranging from 75 to 150 mm wrapped in a filter fabric. PVDs shorten the drainage path in addition to increasing the permeability [29]. The efficacy of this method depends on the drain diameter, spacing, and configuration. However, the overall maintenance cost of these PVDs is high, as they may get clogged and not serve their purpose at times [30, 31].

Grouting involves the injection of low viscous cementitious binders like colloidal silica at high pressures that can bind the sand particles into a hard matrix [32, 33]. The effectiveness of this method depends on the binder being used, permeability of the sand, viscosity, and setting time of the binder. Recently, biocementation using microbially induced calcite precipitation has been verified for its large-scale applicability to mitigate liquefaction [34–36]. However, the leaching of unused chemicals into the groundwater is a serious concern for field applications.

The United Nations Sustainable Development Goals (UN SDG) throw light on the need for sustainable development to reach the needs of the present generation without taking away the ability of future generations to meet their own requirements. Focus is drawn mainly on building sustainable and resilient infrastructure in its Goal 9: Industry, Innovation, and Infrastructure; and Goal 11: Sustainable cities and communities [37]. Hence, finding sustainable alternatives for the above-described liquefaction mitigation techniques to improve the capacity building of future infrastructure is also necessary. Geosynthetics are one such class of materials that established themselves as sustainable and economical alternatives for a wide range of geotechnical applications [38]. The additional confinement and apparent cohesion imparted to the soil by the inclusion of geosynthetics are the primary contributors to the enhanced response of the geosynthetic-reinforced soils [39].

Geotextiles are planar polymeric geosynthetic sheets with significant tensile strength and good drainage characteristics [40]. They are mainly used as tensile reinforcement, filters, and as drainage layers in reinforced soil constructions [41]. These are readily available in the form of rolls which can be spread into sheets and can be placed as layers with adequate spacing in the soil. Several experimental and numerical studies demonstrated the potential of geotextiles for field applicability as inclusion for backfills in retaining walls and slopes [42–45]. The additional confinement and apparent cohesion imparted to the soil due to the mobilization of tensile strength of the geotextile due to sand–geosynthetic interactions add to the liquefaction resistance of the soil [46].

High tensile strength polymeric fibers made of polypropylene are also being used to provide homogeneous and isotropic enhancement in the response of soil structures [47–49]. It was found that the improvement in the response of soils depends on the fiber content and the length of fibers [50, 51]. Recently natural coir fiber from the coconut industry is also being investigated for its capability to reinforce soil structures due to its high tensile strength in the range of 80–120 MPa [52, 53]. This high tensile strength of the fibers can help restrict the lateral movement of the particles during seismic shaking, thereby reducing its potential toward contraction and liquefaction [54].

Geosynthetic-encased granular columns are widely used for improving the bearing capacity of soft grounds and reducing settlements [55]. These are columns of compacted sand or gravel-sized particles confined with geosynthetics like geotextile or geogrids that are inserted into the ground [56]. They are also referred to as stone columns or granular piles. The performance of this method depends on the soil-column load distribution and the modification of the drainage patterns, which in turn depend on the column size and their spacing configurations [57, 58]. Their ability to provide additional stiffness to the soil and allowing quick

dissipation of the pore pressures can be helpful in mitigating liquefaction in soils.

Compressible inclusions like rubber and foam damp the vibrations and increase the resistance of soil against earthquakes [59]. Expanded polystyrene (EPS) geofoam is a lightweight polymeric material with a closed-cellular structure produced by heating EPS beads with steam and then pressing them into prismatic blocks [60]. Due to its lightweight and excellent damping and energy absorption characteristics, geofoam finds its major applications as a substitute for the backfill materials in retaining walls, pavements, and bridge abutments to reduce the self-weight of these structures and also helps in reducing the lateral pressures acting on them [61]. It is also often used as a seismic buffer to dampen the vibrations and absorb the earthquake shocks [62]. Geofoam's ability to compress and dampen the vibrations can be capitalized to increase the liquefaction resistance of sands.

Few studies were carried out to understand the liquefaction response of sands reinforced with these methods [41, 63–66]. However, the effectiveness of these methods and their relative efficacy is not clear and makes it difficult to choose the suitable technique. Hence the objective of the present study is to understand the effectiveness of these sustainable techniques for liquefaction mitigation using geotextile, geofoam, encased granular columns, and coir fibers and compare their efficacy to help geotechnical practicing engineers to choose suitable sustainable techniques depending on the desired improvement for capacity building of soil structures against liquefaction. For this, a series of stress-controlled constant volume cyclic simple shear tests were performed on unreinforced sand and sand with these inclusions, and the test results were compared. The materials used, test methodology, specimen preparation techniques, test program, results obtained, and major conclusions drawn from this study are all described in the subsequent sections.

Materials

Sand

Natural river sand was procured from a local supplier for liquefaction testing. The grain size distribution of the sand, determined as per ASTM D6913 [67], is shown in Fig. 1, along with the microscopic image of the sand particles at 16× magnification. The coefficient of curvature (C_c) and coefficient of uniformity (C_u) of the sand were found to be 1.1 and 3.4, respectively. Well-established and popular morphological descriptors like Wadell's roundness (R) and sphericity (S) and Lees's angularity (A) are determined using image analysis [68–70]. A detailed description of these shape parameters and the steps involved in the shape

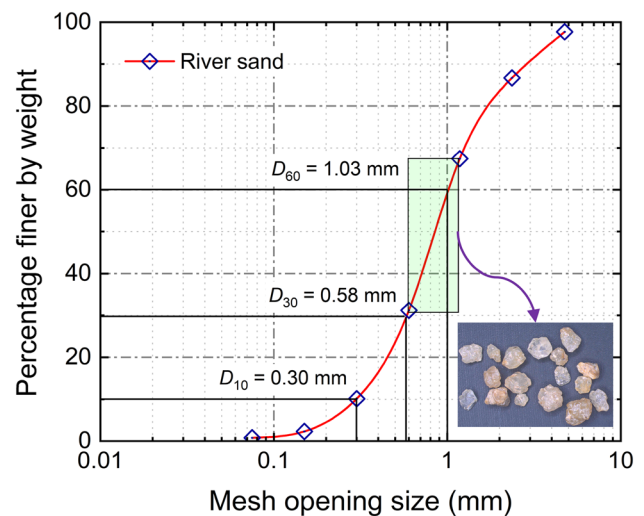


Fig. 1 Grain size distribution of river sand

characterization using image analysis can be found in Latha and Lakkimsetti [21].

From the visual charts of Krumbein and Sloss [71] for grain shape classification, the current sand particles fit into the regime of subrounded grains. The obtained shape features of the sand particles from the image analysis reveal the same, showing high sphericity and low angularity values. River erosion activity is the primary cause of this. According to Unified Soil Classification System (USCS), as per ASTM D2487 [72], this soil falls in the category of poorly graded sand (SP). Sand particles with grain sizes in the range of 0.6 mm and 1.2 mm were scalped out from the sand to obtain uniformly graded sand. This uniformly graded sand with high liquefaction potential was used for liquefaction testing. Physical properties like specific gravity (G_s), minimum void ratio (e_{min}), and maximum void ratio (e_{max}) are determined according to the ASTM D854 [73], ASTM D4253 [74], and ASTM D4254 [75] standards, respectively, and are presented in Table 1 in addition to the computed average shape descriptors of the sand particles.

Materials Used for Liquefaction Mitigation

The efficacy of various sustainable techniques like the inclusion of polymeric geotextile (GTX), mixing of coir fibers (CFS), providing encased granular columns (EGC), and inclusion of geofoam (GFM) for liquefaction mitigation is examined and compared in the present study. The selection of test materials used as inclusions in the present study and their configuration is judicially selected to compare their best possible performance in the field based on the recommendations of literature. For the case of inclusion of polymeric geotextile, a nonwoven geotextile of nominal thickness 1 mm is used. This selection was based on the recommendations

Table 1 Shape descriptors and physical properties of the river sand

Material	Shape descriptors			Physical properties		
	Roundness (R)	Sphericity (S)	Angularity (A)	Specific gravity (G_s)	Minimum void ratio (e_{min})	Maximum void ratio (e_{max})
River sand	0.45	0.85	540	2.61	0.69	0.86

of Krishnaswamy and Isaac [76] and Altun et al. [41], who demonstrated that nonwoven geotextiles perform better when compared to woven geotextiles for liquefaction mitigation due to their excellent drainage characteristics, low elastic modulus, and dense structure. Also, for most engineering applications, nonwoven geotextiles of thickness 0.5 mm to 1.0 mm are commonly used to draw a balance between strength, permeability, and cost.

To bring out the full potential of mixing coir fibers in improving the liquefaction resistance of sands, a coir fiber content of 0.75% was used to reinforce the sand. This is based on the recommendations of Maheshwari et al. [63], Rasouli and Fatahi [77], and Zhou et al. [78], who demonstrated that the liquefaction resistance of sands increases with an increase in the fiber content up to a threshold fiber content of 0.75 to 1% depending on the type of fibers, beyond which ensuring the uniformity and homogeneity of fibers become more difficult. Hence, a coir fiber content of 0.75% is used in the present study. Similarly, for the case of providing encased granular columns, to determine the maximum efficiency of this technique, four encased granular columns arranged in a square configuration resulting in an area replacement ratio (A_r) of 16% are used. This is based on the recommendations of Murugesan and Rajagopal [79], Mohapatra et al. [58], and Castro [80], who demonstrated the beneficial grouping action of square configuration. Also, the chosen A_r value is well within the range of the most widely adopted area replacement ratio, i.e., 5–30% [81, 82].

For the case of inclusion of geofabric layer, although geofabric of various densities in the range of 10–35 kg/m³ is available commercially, a lightweight geofabric of density 12 kg/m³ is chosen in this study. This is based on the recommendations of Wang et al. [83], Zarnani and Bathurst [62], Athanasopoulos-Zekkos et al. [84], and Khan and Meguid [85], who demonstrated that low-density geofabric dampens and reduces the vibrations more effectively due to their excellent compressibility and energy absorbing properties. In the present study, the thickness of geofabric layer is chosen to be 10 mm. Providing a thin layer beyond this thickness is difficult in the field as the flexural strength of the geofabric is very low and can cause damage during transportation and installation.

The details of the test materials used to mitigate liquefaction in sands, along with their properties, are described in the subsequent subsections. Figure 2 shows the photographs of all the materials employed in the current study for liquefaction mitigation, along with the unreinforced river sand included in Fig. 2a.

Inclusion of Polymeric Geotextile

MacTex, a commercially available nonwoven geotextile of nominal thickness 1 mm obtained by needle punching the arbitrarily oriented polypropylene fibers and thermally compressing them into sheets, is used in the present study. A photograph of the nonwoven geotextile used is presented in

Fig. 2 Materials used: **a** natural river sand; **b** geotextile; **c** coir fibers; **d** angular manufactured sand used for encased granular columns; and **e** geofabric

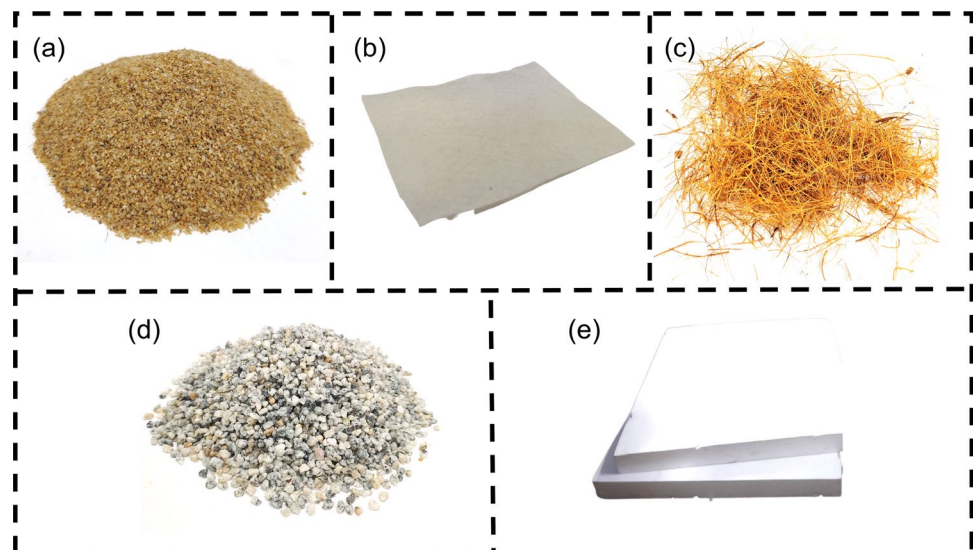


Fig. 2b. Physical properties of the nonwoven geotextile, like ultimate tensile strength, mass per unit area, thickness, and apparent opening size, are determined as per ASTM D4595 [86], ASTM D5261 [87], ASTM D5199 [88], and ASTM D4751 [89] standards, respectively, and are listed in Table 2.

Mixing of Coir Fibers

Coir fibers obtained by mechanical extraction from the fully matured coconuts are procured from a local market. Figure 2c shows the photograph of the coir fibers used in the present study. The average tensile strength of the coir fibers, as per ASTM D3822 [90], was determined using a universal testing machine, and it was found to be 102 MPa. The diameter of the coir fibers varied in the range of 65–500 μm. Original fiber length varied in the range of 25–250 mm. To avoid entanglement of the fibers within the specimen, the fiber length was made sure to be less than the lowest dimension of the specimen by shredding them into shorter lengths. A coir fiber content of 0.75% is chosen in the present study.

Providing Encased Granular Columns

The nonwoven geotextile MacTex that is shown in Fig. 2b, described in the earlier section, was used for providing encasement to the granular columns. Highly angular manufactured sand with coarse-sized particles in the size range of 2.36–4.00 mm obtained by crushing the rock from a nearby quarry is used as the infill material for the granular columns. Figure 2d shows the photograph of the manufactured sand used. The physical properties and shape descriptors are determined for the manufactured sand in line with the procedure described earlier for the river sand and are listed in Table 3. A square configuration of columns is adopted in the present study. The grain size distribution curve of the manufactured sand used, along with the microscopic image of the particles at 16× magnification, is presented in Fig. 3.

Table 2 Physical properties of the geotextile used

Property	Mass per unit area (g/m ²)	Thickness (mm)	Apparent opening size (μm)	Elongation at peak load (%)	Ultimate tensile strength (kN/m)
Value	150	1	100	50	7

Table 3 Shape descriptors and physical properties of the manufactured sand

Material	Shape descriptors			Physical properties		
	Roundness (<i>R</i>)	Sphericity (<i>S</i>)	Angularity (<i>A</i>)	Specific gravity (<i>G_s</i>)	Minimum void ratio (<i>e_{min}</i>)	Maximum void ratio (<i>e_{max}</i>)
Manufactured sand	0.35	0.63	898	2.66	0.69	0.90

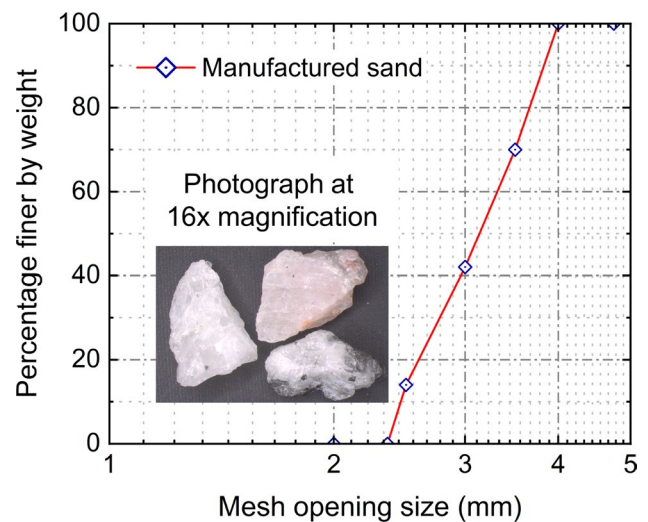


Fig. 3 Grain size distribution of manufactured sand

Inclusion of Geofoam

Geofoams are lightweight fill materials that are commonly used as an alternative to the backfill soil. Commercially, these are available in the form of prismatic blocks. In the present study, prismatic blocks of size 1 × 1 × 0.1 m made of expanded polystyrene (EPS) with a density of 12 kg/m³ are procured from a supplier are used to make geofoam discs that are to be used as an inclusion to mitigate liquefaction in sands. A photograph of the EPS geofoam blocks is shown in Fig. 2e. The physical properties of geofoam are determined as per ASTM D1621 [91] and ASTM D3999 [92] standards from strain-controlled unconfined static and cyclic uniaxial compression tests on geofoam cylinders of 50 mm diameter and 100 mm height. The compressive strength at 10% strain, initial tangent modulus, dynamic modulus of elasticity, bulk modulus, and dynamic shear modulus were found to be 57.5 kPa, 2.4 MPa, 2660 kPa, 1031 kPa, and 1243 kPa, respectively.

Test Methodology

To assess the efficacy of various mitigation techniques under consideration, a series of stress-controlled constant volume cyclic simple shear tests were performed on unreinforced

sand and sand with different inclusions. The detailed description of the cyclic simple shear test setup used, along with its specifications, specimen preparation techniques, and test program, are presented in this section.

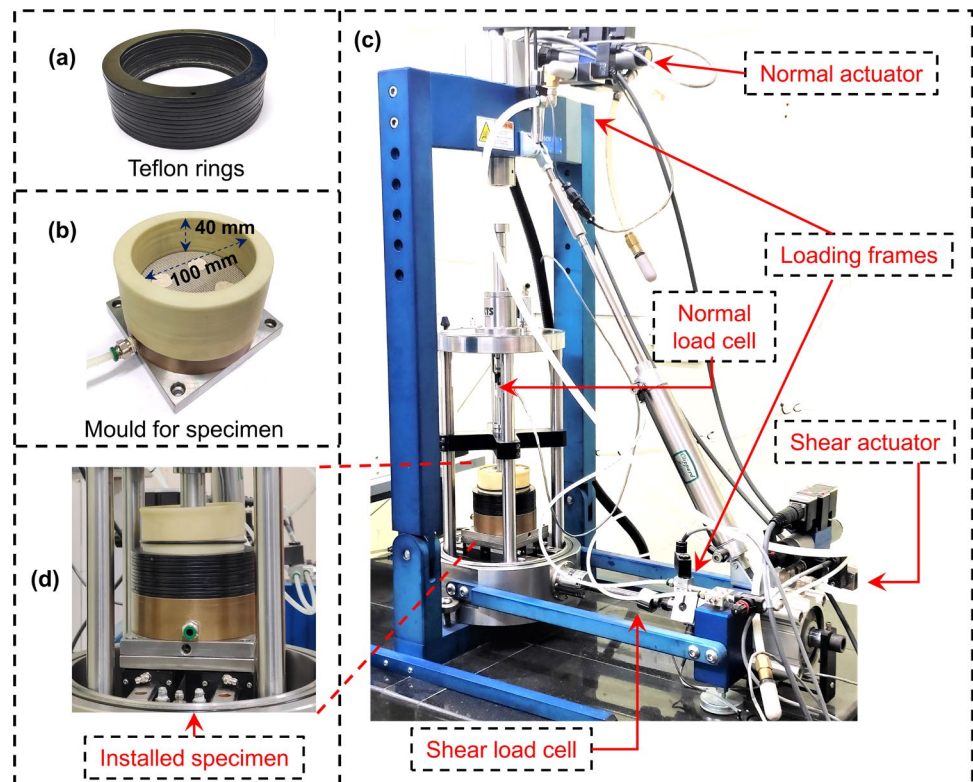
Cyclic Simple Shear Test

Swedish geotechnical and Norwegian geotechnical types are the most commonly used cyclic simple shear tests across the globe for liquefaction testing. In a Swedish geotechnical type, a stack of Teflon-coated rigid rings is used to confine the specimen laterally to guarantee at-rest (K_0) stress conditions by ensuring zero lateral extension of the specimen [66]. Whereas in the case of the Norwegian type, the K_0 stress condition is established with the help of a wire-reinforced latex rubber membrane [93, 94]. The current study uses a Swedish geotechnical type of simple shear test setup available at the Indian Institute of Science Bangalore of GCTS USA make that can accept specimens with a diameter of 100 mm and height of 40 mm. Figure 4 provides a detailed description of the various components of the simple shear test setup, along with the photographs. Figure 4a shows the stack of Teflon rings used. The aspect ratio of the specimen is 0.4 (Fig. 4b) and is well within the permissible limits of the ASTM D8296 [95] to avoid nonuniform stress distributions that result from the absence of counter-shear stresses on the vertical boundaries.

Dyvik et al. [15] performed simple shear tests both under constant volume conditions and truly undrained conditions and demonstrated a good agreement between the test results. Mao and Fahey [17], Porcino et al. [96], and Zhou et al. [66] have also adopted constant volume testing over truly undrained testing due to the simplicity of specimen preparation techniques, and liquefaction tests can be performed on completely dry specimens without the need for saturation. Constant volume conditions can be achieved either using an active or passive height control method. The active height control method involves regulating the vertical stress on the specimen during shearing to maintain a constant height. In the passive height control method, the normal actuator is mechanically clamped and restrained from any movement during the shearing phase to avoid any change in the specimen height.

In the present study, the passive height control method is adopted to ensure constant volume conditions. As seen in Fig. 4c, both the normal actuator and shear actuator are pneumatically controlled and have a loading capacity of 5 kN each with a maximum displacement stroke of ± 12.5 mm. Normal stress (σ) is applied to the specimen with the help of normal actuator, and the shear stress (τ) is transferred from the shear actuator via the sliding bottom platen with the top platen being fixed. Both stress-controlled and strain-controlled tests can be performed, and the test setup is equipped with a sophisticated data acquisition system that records the data automatically. A close view of a typical specimen

Fig. 4 Details of the cyclic simple shear test setup: **a** Teflon rings; **b** mould for the specimen; **c** photograph of the test setup; and **d** close-up view of the installed test specimen



prepared for liquefaction testing installed on the sliding platform with linear bearings is shown in Fig. 4d.

Specimen Preparation

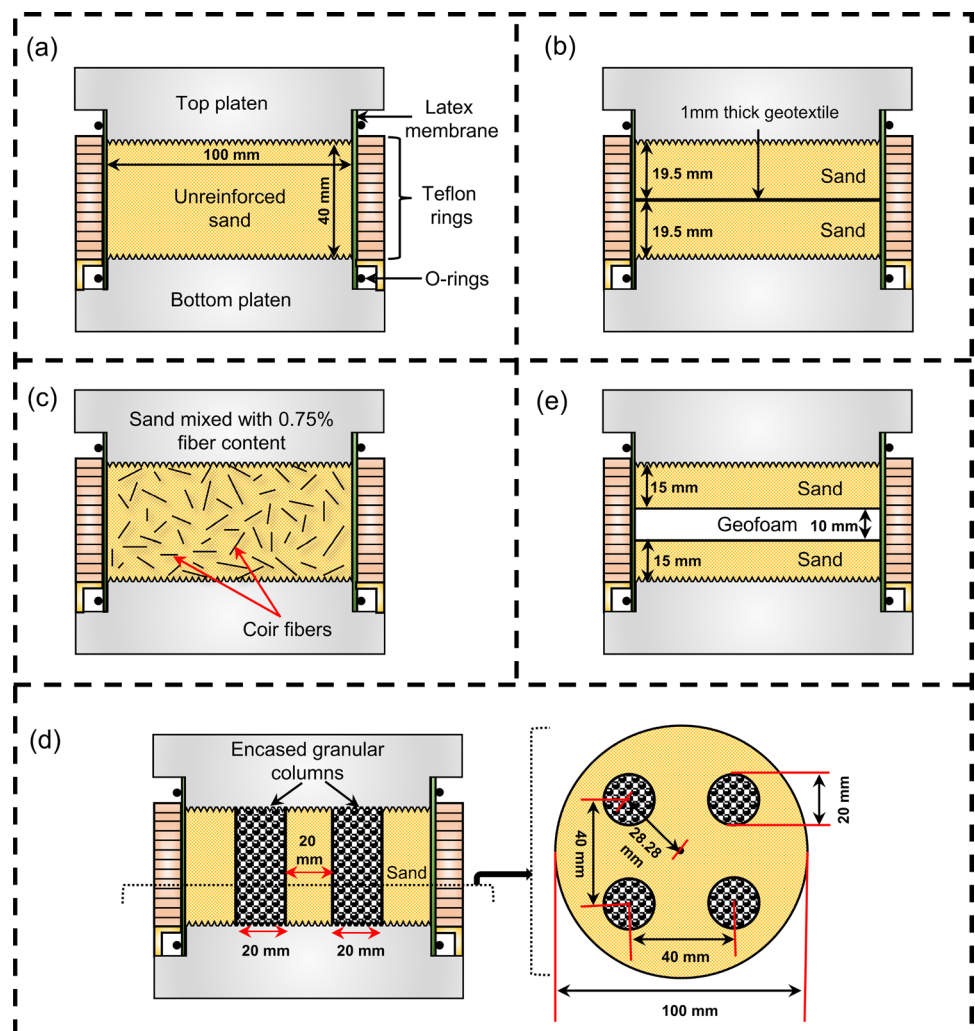
The mould for the specimen preparation with an internal diameter of 100 mm and height of 40 mm, shown in Fig. 4b, is an assembly where the latex rubber membrane is pulled over and inflated to the stack of Teflon rings placed on the bottom platen of the specimen with vacuum assistance and secured with O-rings. The schematic illustration of the specimen preparation techniques and the layout of various inclusions for different mitigation techniques are presented in Fig. 5.

For unreinforced sand specimens, dry pluviation technique was adopted, wherein predetermined weight of river sand is fed into the specimen mould via a hopper from a pre-calibrated height of fall corresponding to the required relative density. Once the mould is filled with the sand, the top surface is leveled, the top platen is placed over it, and the

latex membrane is pulled onto it and secured with an O-ring, as seen in Fig. 5a. For sand specimens with geotextile, one layer of nonwoven geotextile of thickness 1 mm is placed at the mid-height of the specimen, as shown in Fig. 5b. The required amount of river sand is divided into two equal portions and filled into the mould by dry pluviation technique, with geotextile being sandwiched between them.

In the case of fiber-reinforced sands, ensuring uniformity and homogeneity of coir fibers is crucial for maintaining a uniform confinement effect in the sample and attributing the results to a specific volume content. Segregation, entanglement, balling up or clumping of the fibers, and tendency to drag and align close-to-horizontal orientation during mixing oppose our efforts to come up with a homogenous mixture [97–100]. To date, there is no standard procedure for preparing fiber-reinforced sand specimens. Most of the studies recommend thorough manual or automated mixing of fibers with sand having 6 to 10% water content to avoid segregation and also recommend tamping in layers over the dry pluviation method to achieve the desired relative density [77,

Fig. 5 Schematic illustration of the prepared specimens: **a** unreinforced sand; **b** sand with GTX; **c** sand with CFS; **d** sand with EGC; and **e** sand with GFM



99, 101, 102]. Also, the uniform distribution of fibers in a specimen is verified only by visual inspection [97, 100, 103]. Also, based on the estimated number of tests for different cyclic stress ratios (*CSR*), the mixing of fibers with moist sand is usually done in a single batch to ensure uniformity across the specimens, and then, the mixture is dried and stored in bags [78, 101].

Hence, in the present study, the fiber-reinforced sand mixture required for the entire set of experiments (with a fiber content of 0.75% by weight of sand and different *CSR* values) is prepared in one go in a single batch by thoroughly mixing the coir fibers manually with sand having a moisture content of 10% to ensure homogeneity and uniformity within a specimen and across different specimens. This batch of mixture is dried and stored in a container for later usage while preparing the specimens. Test specimens are prepared at the desired relative density by tamping the required quantity of fiber-reinforced sand mixture into 4 layers of equal height, as shown in Fig. 5c.

For the case of encased granular columns, the most commonly adopted area replacement ratio (A_r) in engineering projects is in the range of 5–30% [81, 82]. Area replacement ratio (A_r) is defined as the ratio of cross-sectional area of the installed granular columns to the total cross-sectional area of the treated soil [65]. Also, several studies demonstrated the beneficial effects of a square configuration of columns over other patterns due to the grouping action, enhanced stress concentration, and additional confinement offered to the intervening soil [58, 79, 80]. In the present study, as shown in Fig. 5d, four columns of 20 mm diameter and 40 mm spacing were installed in a square configuration, which corresponds to an area replacement ratio of 16% for a specimen of 100 mm diameter. In the field, this corresponds to a test site of 2×2 m area being reinforced with four encased granular columns of 0.45 m diameter and 1 m spacing installed in a square configuration. Hence the geometric scaling factor adopted in this study turns out to be 22.5. A geometric scaling factor of this order is commonly adopted by several other studies for investigating the performance of encased granular columns in laboratories [104].

Open-ended tubes made of thin steel sheets with an inner diameter of 20 mm equal to the required diameter of the granular column were first lined outside with the tight geosynthetic encasement tubes made of nonwoven geotextile shown in Fig. 2b. These geotextile-encased steel tubes are now erected at desired locations in the empty specimen mould corresponding to the square configuration, as shown in Fig. 5d. Predetermined weight of river sand was then fed via hopper using the dry pluviation technique around the tubes. Manufactured sand shown in Fig. 2d with particle size in the range of 2.36 mm to 4 mm having high angular shape features is used as an infill for the granular columns. Predetermined weight of manufactured sand corresponding

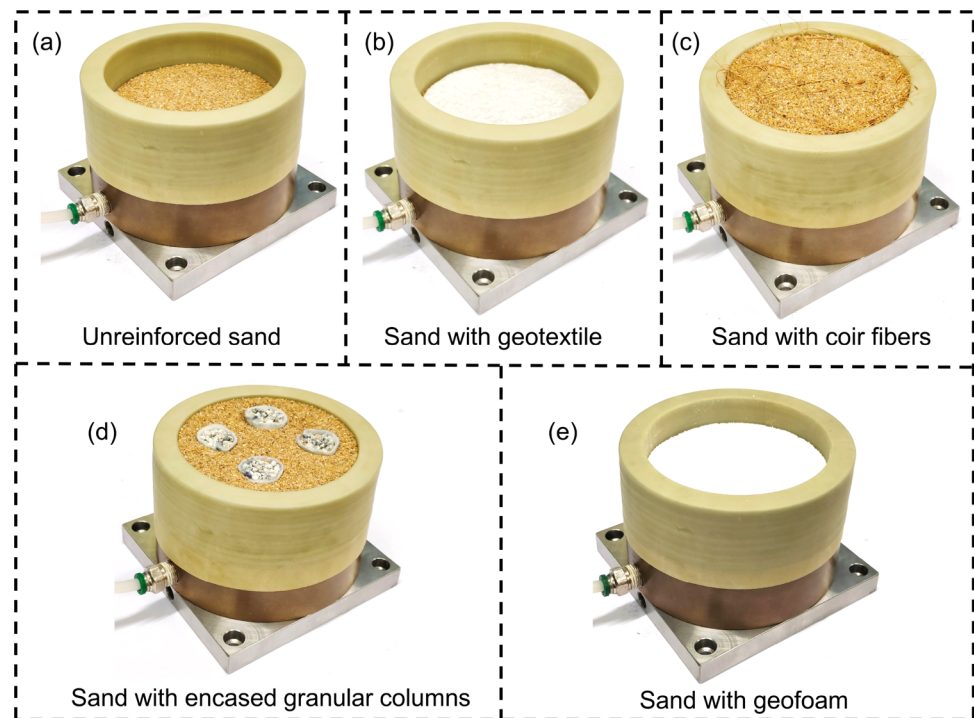
to a relative density of 70% is fed into the tubes in four equal portions and compacted using a tamping rod of diameter 5 mm to accommodate each portion in a height of 10 mm. After compacting each portion of the manufactured sand to a 10 mm-thick layer, the steel tube is gradually withdrawn vertically upwards to the next level of compaction with minimal disturbances to the geosynthetic encasement. The smooth surface of the steel sheet tubes helped in minimized the disturbances during their withdrawal. This process is repeated till the granular columns reach the full height of the specimen.

For sand specimens with geofoam inclusions, EPS geofoam of 12 kg/m^3 density is used. One layer of geofoam of thickness 10 mm is placed at the mid-height of the specimen, as shown in Fig. 5e. Geofoam discs of 100 mm diameter and 10 mm thickness are obtained from the geofoam blocks that are shown in Fig. 2e using hot-wire cutting. The required amount of river sand is divided into two equal portions and filled into the mould by dry pluviation technique, with the geofoam disc being sandwiched between the sand layers. The relative density of river sand in all the specimens is maintained at 30%. The photographs of all the specimens during their reconstitution are shown in Fig. 6.

Test Program

The liquefaction potentials of the specimens made from unreinforced sand and sand with different inclusions were determined by performing a series of stress-controlled constant volume cyclic simple shear tests. Liquefaction testing is performed on completely dry specimens without saturation with water under constant volume conditions as per the ASTM D8296 [95] standard. This way of testing is the most commonly adopted method of determining the liquefaction potential of sands using cyclic simple shear tests [13, 66, 105, 106]. The prepared specimens are now mounted onto the sliding base of the test setup, and an initial effective normal stress (σ'_{n_0}) is applied to the specimen with the help of the normal actuator and left undisturbed till no change in the normal linear variable differential transducer (LVDT) is observed to ensure complete K_0 -consolidation of the specimen. A target relative density of approximately 30% for the river sand is achieved in all the test specimens after K_0 -consolidation. The initial height of the test specimen is kept a bit higher than 40 mm, so that after K_0 -consolidation, the relative density of the specimen reaches 30% for the final specimen dimensions of 100 mm diameter and height of 40 mm. Several studies adopted relative densities in the range of 20–50% to prepare loose specimens for liquefaction testing [107, 108]. The 30% relative density chosen in this study is well within this range. Later, the specimen was sheared cyclically at a constant frequency of 0.20 Hz under stress-controlled constant volume conditions with the help of

Fig. 6 Photographs of the specimens during reconstitution: **a** unreinforced sand; **b** sand with GTX; **c** sand with CFS; **d** sand with EGC; and **e** sand with GFM



the shear actuator, while the normal actuator was mechanically clamped during shearing. Although earthquakes radiate seismic waves within the frequency of 0.01–10 Hz, most of the element testing for determining the liquefaction potential of sands was conducted within a low-frequency range of 0.1–1 Hz [13, 105, 109]. This is done to avoid discrepancies in the recording of pore pressures and ensure enough time for the stabilization and uniform distribution of the pore pressure within the test specimens. The frequency value used in the study corresponds to a low-frequency earthquake.

The building up of pore pressure during cyclic shearing decreases the effective normal stress during any cycle N_c ($\sigma'_{n_{Nc}}$) that is holding the grain contacts gradually as the shearing continues. After a certain number of cycles, the effective normal stress ($\sigma'_{n_{Nc}}$) drops to zero with the grain contacts being completely broken, and the specimen is treated to be completely liquified at this stage. The number of cycles needed for complete liquefaction (N_f) is recorded for each test specimen and is related to its liquefaction resistance. Higher the value of N_f , greater is the liquefaction resistance of the specimen. Pore pressure ratio (r_u), which is defined as the ratio of excess pore pressure ($\sigma'_{n_0} - \sigma'_{n_{Nc}}$) to the initial effective normal stress (σ'_{n_0}), is the most commonly used parameter in the liquefaction studies. The value of r_u becoming unity indicates complete liquefaction. The ratio of applied cyclic shear stress (τ) to the initial effective normal stress (σ'_{n_0}) is referred to as the cyclic stress ratio (CSR). Four cyclic stress ratios (CSR) in the range of 0.125–0.250 are chosen for obtaining the liquefaction resistance curves for the unreinforced sand and

sand with different inclusions. The CSR values adopted for liquefaction testing in the present study are within the range of 0.1 to 0.5, which are commonly used by several researchers for determining the liquefaction resistance of reinforced sands [108, 110]. Different CSR values are adopted for unreinforced sand and sand with different inclusions as they have different liquefaction resistances. This way of choosing different CSR values for sands with different inclusions to obtain liquefaction resistance curves is also adopted in many earlier studies in the literature [34, 76]. Table 4 presents the summary of cyclic simple shear tests performed along with the recorded N_f values for each test. The values of N_f obtained for sand with various inclusions are in line with the values obtained by earlier studies on liquefaction resistance of unreinforced and reinforced sands [34, 66, 105].

Results and Discussion

To evaluate the effectiveness of the considered techniques for liquefaction mitigation, test results from the cyclic simple shear tests on unreinforced sand and sand with different inclusions are compared and interpreted in terms of the liquefaction resistance curves, pore pressure response, shear strain accumulation, stress–strain response, modulus degradation, stress path followed, and strain energy dissipated, in this section.

Table 4 List of cyclic simple shear tests conducted

S. no	Material	CSR	N_f
1	Unreinforced sand	0.125	94
2	Unreinforced sand	0.1375	68
3	Unreinforced sand	0.15	29
4	Unreinforced sand	0.175	9
5	Sand with GTX	0.125	342
6	Sand with GTX	0.15	82
7	Sand with GTX	0.175	30
8	Sand with GTX	0.20	15
9	Sand with CFS	0.125	490
10	Sand with CFS	0.15	260
11	Sand with CFS	0.175	65
12	Sand with CFS	0.20	28
13	Sand with EGC	0.125	620
14	Sand with EGC	0.15	300
15	Sand with EGC	0.175	126
16	Sand with EGC	0.20	80
17	Sand with GFM	0.15	530
18	Sand with GFM	0.175	265
19	Sand with GFM	0.20	130
20	Sand with GFM	0.25	34

Liquefaction Resistance Curves and Pore Pressure Response

Stress-controlled constant volume cyclic simple shear tests were performed on specimens made from unreinforced sand and sand with different inclusions with four different CSR values ranging from 0.125 to 0.250, and the liquefaction resistance of the materials is expressed in terms of the number of cycles (N_f) needed for complete liquefaction of the specimen. The specimens are treated to be liquefied when the r_u value becomes unity (i.e., effective normal stress becomes zero). The plots between CSR and corresponding N_f values are referred to as the liquefaction resistance curves. Saxena et al. [111] correlated CSR with N_f by performing regression analysis on large test data from simple shear tests, as shown in Eq. 1, where a and b are the regression coefficients

$$CSR = a \times N_f^{-b} \tag{1}$$

This equation was adopted in several studies to obtain the liquefaction resistance curves [34, 77]. The values of N_f for corresponding CSR values from all the tests performed are listed in Table 4. The liquefaction resistance curves for the unreinforced sand and sand with different inclusions are shown in Fig. 7, and the associated regression coefficients a and b for the tested materials with a coefficient of determination (R^2) greater than 0.95 are summarized in Table 5.

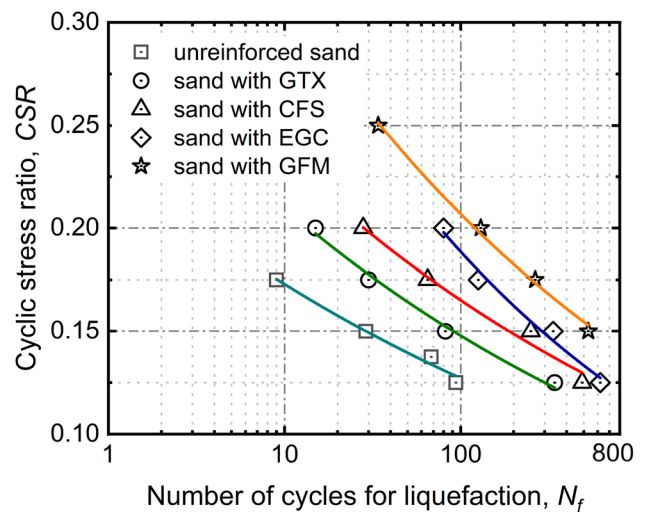


Fig. 7 Liquefaction resistance curves of the tested materials

From Fig. 7, it can be seen that there is a good agreement between the test data and the Saxena et al. [111] model for the liquefaction resistance curves.

The effectiveness of the various mitigation techniques adopted in the current study is brought out by comparing the test results of specimens made from unreinforced sand and sand with different inclusions subjected to the same cyclic shearing at a frequency of 0.2 Hz with a CSR value of 0.175. The pore pressure response of the different test specimens for this loading is presented in Fig. 8. It shows the variation of the pore pressure ratio (r_u) as the cycles progress. It can be seen that the unreinforced sand specimen liquefied in nine cycles as the r_u value reached unity. Whereas the number of cycles (N_f) needed for liquefaction was found to be 30, 65, 126, and 265 cycles, respectively, for sand specimens with GTX, CFS, EGC, and GFM. The inclusion of one layer of nonwoven geotextile increased the liquefaction resistance by 233%. Mixing of 0.75% coir fibers increased the liquefaction resistance by 622%. Providing four encased granular columns of 20 mm diameter each, in a square configuration, gave an improvement in the liquefaction resistance by 1300%. Whereas the inclusion of one layer of 10 mm-thick

Table 5 Coefficients a and b of the liquefaction resistance curves for the tested materials

Material	$CSR = a \times N_f^{-b}$	
	a	b
Unreinforced sand	0.24	0.13
Sand with GTX	0.30	0.15
Sand with CFS	0.33	0.15
Sand with EGC	0.50	0.21
Sand with GFM	0.44	0.16

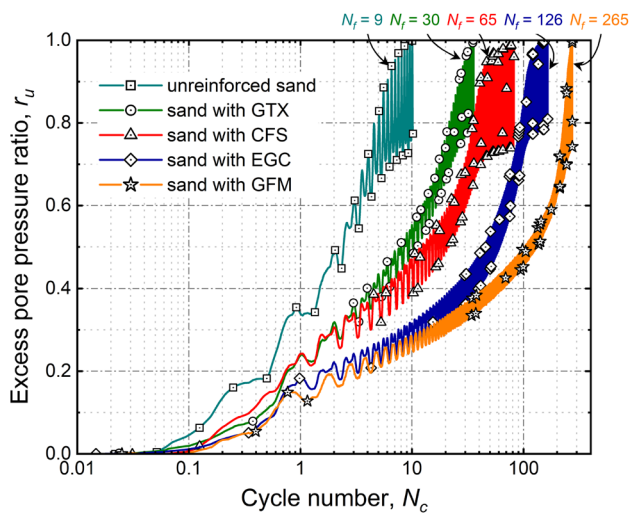


Fig. 8 Pore pressure response of the specimens (CSR of 0.175)

geofoam of density 12 kg/m³ provided a maximum improvement in the liquefaction resistance by 2840% when compared with that of the unreinforced specimen.

Accumulation of Shear Deformations

During the liquefaction, as the specimen loses its shear strength, the shear deformations start accumulating rapidly in the specimen. This shear strain accumulation during liquefaction is responsible for the damages like lateral spreading. Hence, when proposing a mitigation technique, their ability to arrest these shear strains (γ) is of utmost importance from the perspective of serviceability [66]. The shear deformation in the test specimen is measured by the shear LVDT of the test setup, and the shear strain in Fig. 9 is the ratio of shear displacement to the height of the test specimen. In this study, liquefaction tests were performed under constant volume conditions using passive height control method. Hence, there is no change in the height and volume of the test specimen. Hence, the volumetric strain in the test specimens is zero.

Figure 9 presents the shear strain accumulations in the specimens constituted with unreinforced sand and sand with different inclusions when subjected to identical cyclic loading of CSR 0.175. It can be seen that all the suggested mitigation techniques were able to arrest the shear deformations for a large number of cycles when compared to that of the unreinforced specimen. However, the maximum benefit in controlling the shear strains is obtained with the inclusion of the geofoam layer. For instance, let us consider the number of cycles ($N_{DA,5\%}$) needed for the specimen to accumulate a double-amplitude shear strain (γ_{DA}) of 5%. It can be seen that the $N_{DA,5\%}$ values were found to be 7, 24, 43, 111, and 249 cycles, respectively, for unreinforced sand, sand with

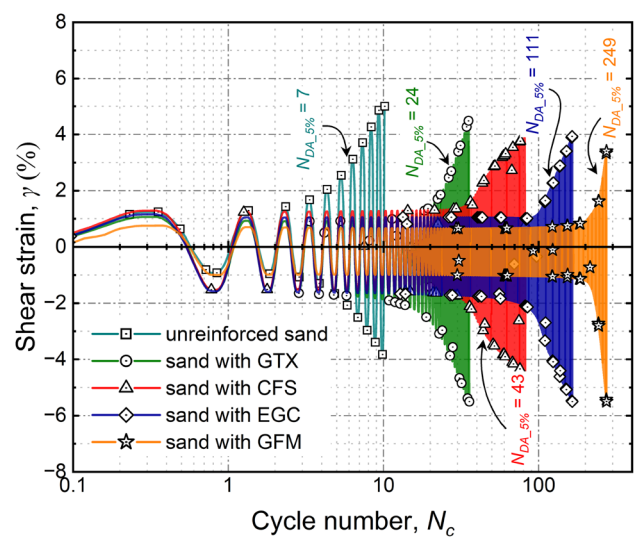


Fig. 9 Shear strain accumulation in the specimens (CSR of 0.175)

GTX, CFS, EGC, and GFM inclusions. The ability to arrest the shear deformations increased by three times for the case of sand with geotextile inclusion. Whereas it is around 6, 15, and 35 times, respectively, for the case of sand with coir fibers, encased granular columns, and geofoam inclusions.

The bulk modulus of geofoam was measured as 1031 kPa. Although geofoam is deformable, due to constant volume conditions being imposed on the test specimen, there is no volumetric strain in the geofoam inclusions during cyclic shearing. The building up of pore pressures during liquefaction reduces the effective stresses that are holding the grain contacts. This results in the reduction of shear strength of the material and leads to the accumulation of larger shear strains for the same applied cyclic shear stress. Since the inclusion of geofoam prevents the development of pore pressures for large number of cycles, as shown in Fig. 8, the rate of reduction in effective stress that is holding the grain contacts is much slower when compared to other techniques adopted in this study. Hence, the strain accumulation in the case of specimens with geofoam inclusions is much less when compared to other techniques used in the present study.

Stress Path Response

During liquefaction testing, the effective normal stress (σ'_n) drops continuously due to the build-up of pore pressure in the specimen. As a result, once the specimen liquefies, it cycles around the critical state line with minimal shear strength. Stress paths are very helpful in tracing the stresses on the specimen during cyclic shearing. The normalized stress path, i.e., CSR vs. normalized effective normal stress being followed by all the test specimens during the eighth cycle of the cyclic loading with a CSR value of 0.175, is

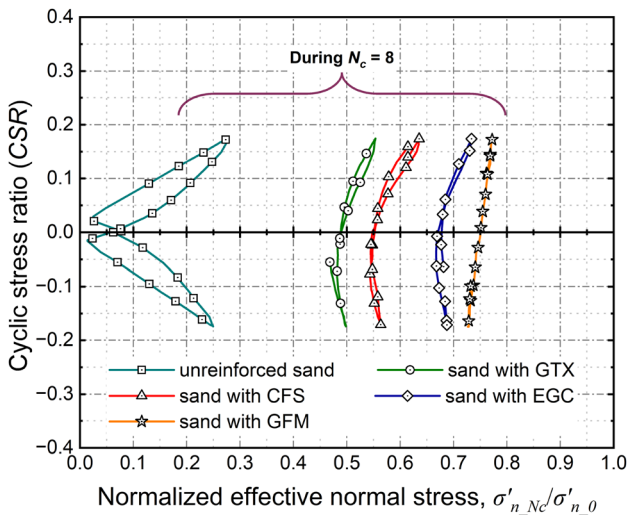


Fig. 10 Stress path followed by the specimens during the eighth cycle of shearing (*CSR* of 0.175)

shown in Fig. 10. Normalized effective normal stress is defined as the ratio of effective normal stress on the specimen during the current cycle N_c ($\sigma'_{n_{Nc}}$) to the initial effective normal stress (σ'_{n_0}). It can be seen that the unreinforced specimen reached the critical state with normalized effective normal stress being dropped to almost zero. The liquefaction mitigation techniques adopted in this study delayed the specimen from reaching its critical state. This is evident from the fact that the normalized effective normal stress dropped only to a value of 0.49, 0.55, 0.68, and 0.75, respectively, for sand with GTX, CFS, EGC, and GFM inclusions after eight cycles of shearing. Geofom delayed the effective normal stress reduction on the specimen by a maximum extent when compared to other techniques.

Stress–Strain Response and Modulus Degradation

Secant shear modulus (G_{sec}) is an important parameter in designing soil structures subjected to dynamic loads. This is usually obtained from the stress–strain response of the specimen. ASTM D8296 [95] adopts the usage of Eq. 2 for obtaining the secant shear modulus of the specimen from cyclic simple shear tests, where τ_a and τ_b are the maximum, and minimum cyclic shear stresses and γ_a and γ_b are the corresponding shear strains. The cyclic shear stress (τ) is the product of *CSR* and the initial effective normal stress (σ'_{n_0})

$$G_{sec} = \frac{\tau_a - \tau_b}{\gamma_a - \gamma_b} \tag{2}$$

Figure 11 shows the normalized stress–strain response of the unreinforced sand and sand with different inclusions during a particular cycle of loading during cyclic shearing

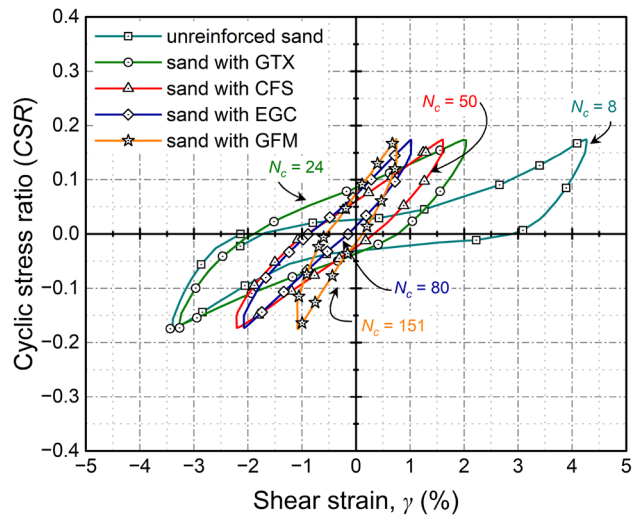


Fig. 11 Stress–strain response of the specimens for a particular cycle of shearing (*CSR* of 0.175)

with a *CSR* of 0.175. All the materials showed a hysteretic response, while the loops widened more rapidly in the case of unreinforced sand. It can be seen from Fig. 11 that the hysteresis loop of unreinforced sand is spread over large shear strains in the range of -3.5 to 4.25% during the 8th cycle. For sand with GTX inclusion, the loop is spread from -3.3 to 2.0% shear strains during the 24th cycle. Whereas for the case of sand with CFS, the 50th cycle loop is within the bounds of -2.2 to 1.5% shear strains. These bounds are -2.0 to 1.0% for the 80th cycle in the case of sand with EGC. Even after 150 cycles of shearing, the hysteresis loops are within the bounds of -1 to 0.75% shear strains for the case of sand with GFM inclusion. These findings suggest that the shear modulus degradation is more rapid in the case of unreinforced sand.

During the undrained cyclic shearing, the secant shear modulus (G_{sec}) drops continuously as the positive pore pressure builds up. This degradation of G_{sec} during liquefaction can be quantified using the degradation index (δ) coined by Idriss et al. [112] and can be computed using Eq. 3, where $G_{sec_{Nc}}$ is the secant shear modulus during the current cycle (N_c), and G_{sec_1} is the secant shear modulus during the first cycle. Several studies have adopted this parameter δ to quantify the cyclic stiffness degradation in unreinforced and reinforced specimens [77, 113, 114],

$$\delta = \frac{G_{sec_{Nc}}}{G_{sec_1}} \tag{3}$$

The cyclic stiffness degradation quantified in terms of the degradation index (δ) for the unreinforced sand and sand with different inclusions during the cyclic shearing with an amplitude of *CSR* 0.175 is shown in Fig. 12. The liquefaction mitigation techniques that are considered in the present

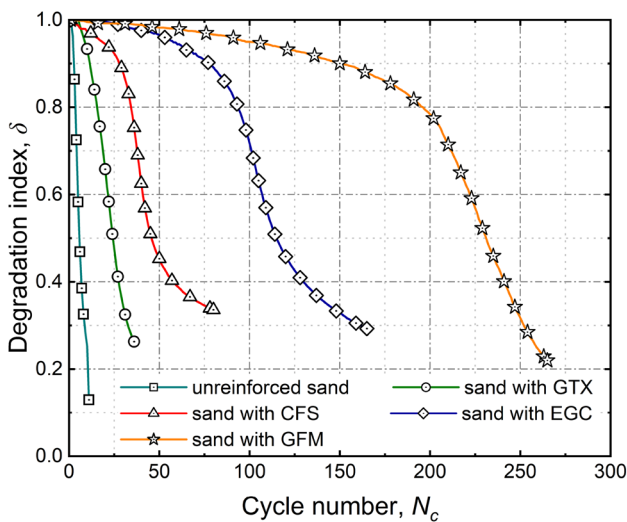


Fig. 12 Secant shear modulus degradation in the specimens (CSR of 0.175)

study were able to delay the shear modulus degradation, with the maximum benefit in the case of sand with GFM inclusion. For the cyclic secant shear modulus to drop by 50% of its initial value (i.e., to reach a δ value of 0.5), the number of cycles required ($N_{\delta_{0.5}}$) was found to be 6, 24, 45, 115, and 231 cycles, respectively, for unreinforced sand, sand with GTX, CFS, EGC, and GFM inclusions. Shear modulus and its degradation are extremely crucial for designing the reinforced geostructures. The detailed quantitative description of the degradation of shear modulus and the comparisons made in this section are beneficial to practicing engineers in selecting suitable techniques depending on the stiffness requirements of the soil structures.

Dissipation of Strain Energy

The grain contacts are broken during liquefaction by consuming tremendous strain energy. The liquefaction resistance of a specimen is directly proportional to the cumulative strain energy dissipated per unit volume of the test specimen (ΔW) during cyclic shearing. The amount of strain energy dissipated (ΔW) in a cycle is essentially equal to the area inside the hysteresis loop [115, 116]. ΔW at any point ‘ i ’ during the shearing with a total of ‘ n ’ data points can be computed using Eq. 4, which was developed by Figueroa et al. [115], where τ and γ are the associated shear stresses and strains. Equation 4 essentially calculates the area inside the hysteresis loop irrespective of the nature of the loop [116]. Several studies have verified and adopted this equation for determining the strain energy consumed during liquefaction irrespective of the nature of the hysteresis loops [51, 117–124]. Figure 13 presents the normalized dissipated strain energy (i.e., the ratio of ΔW computed from Eq. 4 to

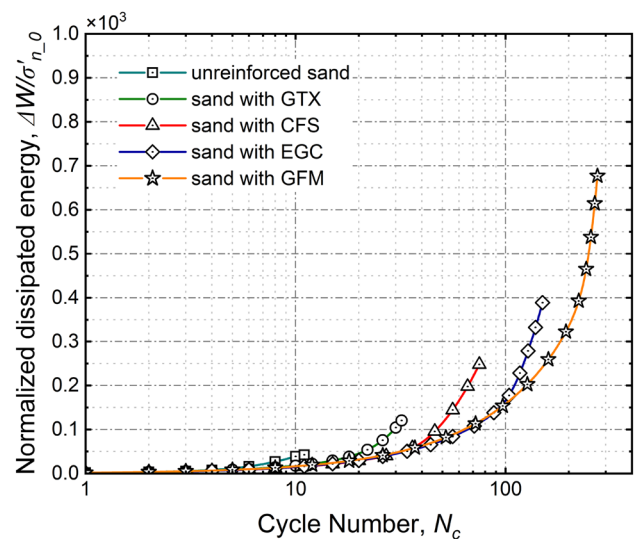


Fig. 13 Normalized dissipated energy in the specimens during cyclic shearing (CSR of 0.175)

the initial effective normal stress) in the case of unreinforced sand and sand with different inclusions during cyclic shearing with a CSR value of 0.175

$$\Delta W = \sum_{i=1}^{n-1} \frac{1}{2} (\tau_i + \tau_{i+1}) (\gamma_{i+1} - \gamma_i) \tag{4}$$

It can be seen from Fig. 13 that the amount of normalized strain energy needed for the unreinforced specimen to break all the grain contacts and liquify is only 42. Whereas with the provision of additional inclusions, the amount of normalized strain energy needed to be dissipated before liquefaction increased, with a maximum value for the case of sand with GFM inclusion. The normalized strain energies dissipated before liquefaction were found to be 120, 248, 389, and 677, respectively, for sand with GTX, CFS, EGC, and GFM inclusions.

Governing Mechanisms and Practical Implications

In the present study, the improvement in the liquefaction resistance of sand was found to be 233%, 622%, 1300%, and 2844%, respectively, for sand with GTX, CFS, EGC, and GFM. Krishnaswamy and Isaac [76], Altun et al. [41], Moayed and Alibolandi [125], and Su et al. [126] reported an improvement in the liquefaction resistance of 275%, 200%, 275%, and 180%, respectively with the inclusion of nonwoven geotextile. The observed 233% improvement with the inclusion of nonwoven geotextile falls in line with these previously reported values. Based on the type of fiber and sand used, Noorzad and Amini [127], Chegenizadeh et al.

[128], Ghadr et al. [129], Zhang et al. [101], Rasouli and Fatahi [77], and Zhou et al. [66] reported an increase in the liquefaction resistance by 275%, 160%, 206%, 820%, 825%, and 655%, respectively. The observed 622% increase in the liquefaction resistance is well within this previously reported range. Studies on the inclusion of encased granular columns for liquefaction mitigation are based on the model tests like shaking table and centrifuge tests and talks only about the qualitative improvement in the response in terms of the reduction in the lateral displacements [65, 130–132]. No study was performed till date to quantify the actual improvement in the liquefaction resistance of sands using this technique. This study quantified the improvement in the liquefaction resistance using encased granular columns to be 1300%. Till date, no study explored the inclusion of geofoam layer for liquefaction mitigation. Present study explored this gap in the literature and an improvement in the liquefaction resistance using geofoam inclusion was found to be 2844%. Results from the present study confirm the potential application of geofoam inclusions for liquefaction mitigation.

Figure 14 compares the effectiveness of various techniques adopted in this study for liquefaction mitigation, where N_f , $N_{DA_{5\%}}$, and $N_{\delta_{0.5}}$ represent the number of cycles required, respectively, for complete liquefaction, double-amplitude shear strain accumulation of 5%, and modulus degradation by 50%. Also, it shows the normalized dissipated strain energies ($\Delta W/\sigma'_{n,0}$) for each technique adopted. Overall, it can be seen from Fig. 14 that the proposed mitigation techniques, i.e., the inclusion of geotextile, mixing of coir fibers, providing encased granular columns, and inclusion of geotextile, have shown positive outcomes in terms of increasing the liquefaction resistance by increasing the amount of cumulative strain energy to be dissipated. Also, they helped in delaying the building up of pore pressures, accumulation of shear strains, and modulus degradation. The improved capacity to resist liquefaction is attributed to the increase in confinement by the action of interface shear strength, which induces apparent cohesion in the case of

sand with geotextile, higher resistance offered to the lateral movement of soil particles in the case of sand with coir fibers, increase in the stiffness of the intervening soil for the case of sand with encased granular columns, and higher compressibility and energy absorption characteristics in the case of sand with geofoam. Figure 15 presents the schematic illustration of these internal mechanisms governing the improved response in different techniques adopted in the present study.

As seen in Fig. 15a, in the case of specimens with geotextile inclusions, the shear stresses developed at the sand–geotextile interfaces mobilize the tensile strength of the geotextile. This results in an increase in the confinement and prevents the lateral rearrangement of particles, thereby improving the liquefaction resistance of sand. In the case of sand reinforced with coir fibers, the improved liquefaction resistance is contributed by the additional 3D confinement provided by the tensile forces developed in the coir fibers. The tensile strength of coir fibers gets mobilized due to the pull exerted by the sand particles upon cyclic shearing, as shown in Fig. 15b. The governing mechanism responsible for the improved response in the case of sand with encased granular columns is demonstrated in Fig. 15c. Due to modulus contrast, the normal stress shared by the columns (σ_c) is much higher compared to the normal stress on the sand (σ_s), causing stress concentration in granular columns. The improved liquefaction resistance is a collective result of grouping action, stress concentration, and additional confinement provided by the columns to the intervening soil. As shown in Fig. 15d, in the case of sands with geofoam inclusions, geofoam absorbs the strain energy and dampens the cyclic stress amplitude τ_{cyc} , thereby delaying the building up of pore pressure. The excellent energy absorption characteristics and ability to dampen the vibrations put the geofoam inclusions one step ahead of the other techniques adopted in the present study for liquefaction mitigation.

It is acknowledged that these methods are suitable only for new constructions to be built with high liquefaction

Fig. 14 Comparison of performance of various liquefaction mitigation techniques adopted

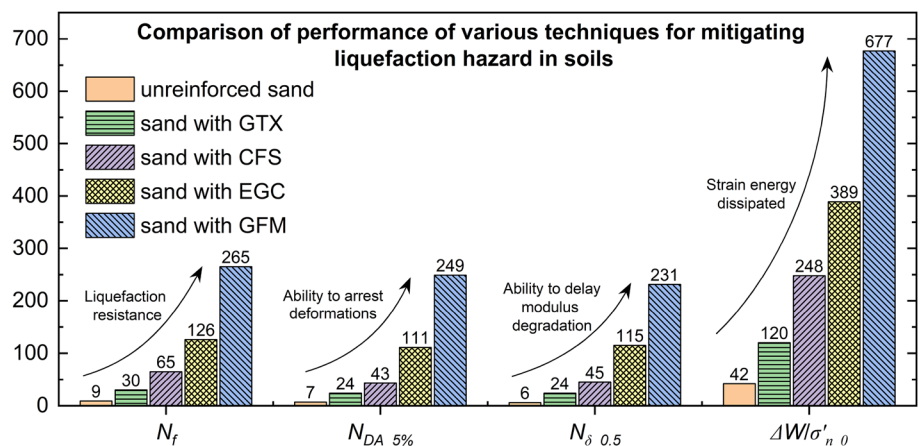
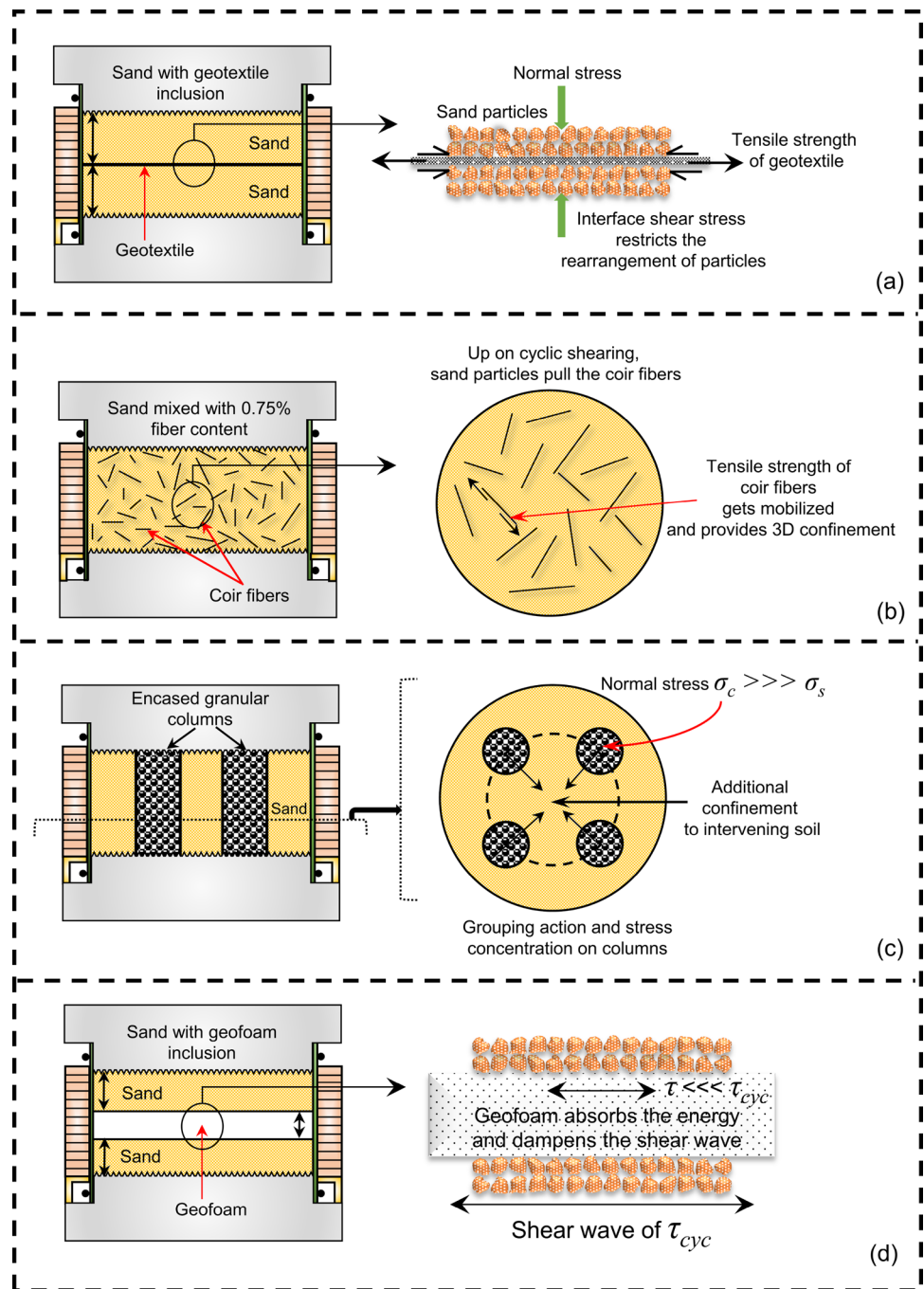


Fig. 15 Schematic illustration of the governing mechanisms for the improved response in each technique



resistance. The performance of these methods follows the order of Geofoam > Encased granular columns > Coir fibers > Geotextile. Geofoam inclusion showed the maximum benefit for liquefaction mitigation among all the methods considered. Geofoam is a highly durable material that can withstand a range of environmental conditions and can maintain its performance over a long period of time. This reduces the need for frequent maintenance or replacement, resulting in a lower environmental impact. The use of geofoam can reduce the need for natural resources such

as soil or rock, which are typically used in construction. This reduces the environmental impact associated with the extraction, transportation, and processing of these materials. Geofoam is a lightweight material, which means that it requires less energy to transport and install. Geofoam is not biodegradable, but it can be recycled at the end of its service. Hence, the use of geofoam can be an environmentally sound choice in comparison to the other techniques. Test results from this study are beneficial for practicing geotechnical engineers and can be directly applied in the field to choose

and implement a suitable sustainable liquefaction mitigation technique with the help of these materials depending upon the desired improvement to be achieved.

Conclusions

The present study examines the efficacy of various sustainable techniques like the inclusion of geotextile (GTX), mixing of coir fibers (CFS), providing encased granular columns (EGC), and inclusion of geofoam (GFM) for mitigating liquefaction in sands through a series of stress-controlled constant volume cyclic simple shear test. Tests were conducted on specimens reconstituted with unreinforced sand and sand with different inclusions, and the results were compared and interpreted in terms of the pore pressure response, shear strain accumulations, modulus degradation, and strain energy dissipated. The following major conclusions can be drawn from these comparisons:

- All the sustainable mitigation techniques considered in this study were able to improve the performance of sand against liquefaction. However, their efficacies were found to be different. A suitable method for the desired improvement in the response can be chosen accordingly.
- For cyclic loading with a cyclic stress ratio (CSR) of 0.175, the number of cycles (N_p) needed for liquefaction (i.e., pore pressure ratio reaching a value of unity) was found to be 9, 30, 65, 126, and 265 cycles, respectively, for unreinforced sand, sand with GTX, CFS, EGC, and GFM inclusions. Liquefaction resistance increased by 233, 622, 1300, and 2840%, respectively, for sand with GTX, CFS, EGC, and GFM inclusions.
- The proposed methods were able to arrest the shear deformations in the specimen. This can be helpful in avoiding lateral spreading and its associated deformations during liquefaction. For a CSR of 0.175, the number of cycles needed for 5% double-amplitude shear strain ($N_{DA5\%}$) was found to be 7, 24, 43, 111, and 249 cycles, respectively, for unreinforced sand, sand with GTX, CFS, EGC, and GFM inclusions. Geofoam increased the ability to arrest the shear deformations in the specimen by 35 times when compared to that of the unreinforced sand.
- Secant shear modulus (G_{sec}) degradation was found to be delayed with the help of all the techniques adopted in this study. For a CSR of 0.175, the number of cycles needed for the shear modulus to drop to half of its initial value was found to be 6, 24, 45, 115, and 231 cycles, respectively, for unreinforced sand, sand with GTX, CFS, EGC, and GFM inclusions. Maximum retardation in the degradation of G_{sec} was found to be in the case of sand with GFM inclusion.

- The strain energy dissipated (ΔW) during cyclic shearing was found to be 5, 15, 29, 55, and 91 kJ/m³, respectively, for unreinforced sand, sand with GTX, CFS, EGC, and GFM inclusions. This shows that breakage of grain contacts is more difficult in the case of reinforced test specimens. Sand specimens with geofoam as inclusion required the maximum amount of strain energy to break the grain contacts highlighting its ability to improve the liquefaction resistance by many folds when compared to other techniques.
- The improved ability to resist liquefaction is attributed to higher compressibility and energy absorption characteristics in the case of geofoam, increased stiffness of the intervening soil in the case of encased granular columns, higher resistance to lateral movement of particles in the case of coir fibers, and increase in confinement by the action of interface shear strength which induces apparent cohesion in case of geotextile.
- Overall, the efficacy of the adopted inclusions follows the order of Geofoam > Encased granular columns > Coir fibers > Geotextile. Test results from this study are helpful for practicing engineers to choose and implement these techniques to improve the capacity building of soil structures against liquefaction.

Acknowledgements The GCTS USA make cyclic simple shear test setup for the liquefaction testing is procured with the Phase 3 financial assistance received from the Department of Science and Technology DST-FIST, Government of India to the Department of Civil Engineering, Indian Institute of Science Bangalore. The microscope employed for the shape characterization of granular materials using image analysis was procured from the SERB POWER fellowship (SPF/2021/000041) of the second author. The financial support received from these organizations is gratefully acknowledged.

Author Contributions BL and GML contributed to the conceptualization and design of experiments. All the experiments were conducted by BL. Test results were analyzed and interpreted by BL and GML. The original draft of the manuscript is written by BL. GML contributed to the editing the draft and supervising. All authors carefully read and approved this version of the manuscript.

Funding The cyclic simple shear test setup used in the present study for liquefaction testing was procured with the Phase 3 financial assistance received from the Department of Science and Technology DST-FIST, Government of India to the Department of Civil Engineering, Indian Institute of Science Bangalore. The microscope employed for the shape characterization of granular materials using image analysis was procured from the SERB POWER fellowship (SPF/2021/000041) of the second author.

Data Availability Data will be made available on a reasonable request.

Declarations

Conflict of Interest The authors declare that they have no competing financial interests or personal relationships that could have appeared to influence the work reported in this paper.

References

- Ainuddin S, Routray JK (2012) Earthquake hazards and community resilience in Baluchistan. *Nat Hazards* 63:909–937. <https://doi.org/10.1007/s11069-012-0201-x>
- Sonmez B, Ulusay R, Sonmez H (2008) A study on the identification of liquefaction-induced failures on ground surface based on the data from the 1999 Kocaeli and Chi-Chi earthquakes. *Eng Geol* 97(3–4):112–125. <https://doi.org/10.1016/j.enggeo.2007.12.008>
- Bhattacharya S, Hyodo M, Nikitas G, Ismael B, Suzuki H, Lombardi D, Egami S, Watanabe G, Goda K (2018) Geotechnical and infrastructural damage due to the 2016 Kumamoto earthquake sequence. *Soil Dyn Earthq Eng* 104:390–394. <https://doi.org/10.1016/j.soildyn.2017.11.009>
- Yang B, Hou J, Zhou Z, Gou J (2023) Failure behavior and mechanism of a slope under the action of earthquake after rainfall. *Nat Hazards* 30:1–8. <https://doi.org/10.1007/s11069-023-05831-3>
- Maurer BW, Green RA, Cubrinovski M, Bradley BA (2015) Fines-content effects on liquefaction hazard evaluation for infrastructure in Christchurch, New Zealand. *Soil Dyn Earthq Eng* 76:58–68. <https://doi.org/10.1016/j.soildyn.2014.10.028>
- Hazarika H, Rohit D, Pasha SM, Maeda T, Masyhur I, Arsyad A, Nurdin S (2021) Large distance flow-slide at Jono-Oge due to the 2018 Sulawesi Earthquake. *Indonesia Soils Found* 61(1):239–255. <https://doi.org/10.1016/j.sandf.2020.10.007>
- Upadhyaya S, Green RA, Rodriguez-Marek A, Maurer BW (2023) True liquefaction triggering curve. *J Geotech Geoenviron Eng* 149(3):04023005. <https://doi.org/10.1061/JGGEFK.GTENG-11126>
- Castro G (1975) Liquefaction and cyclic mobility of saturated sands. *J Geotech Eng Div* 101(6):551–569. <https://doi.org/10.1061/AJGEB6.0000173>
- Ishihara K, Tatsuoka F, Yasuda S (1975) Undrained deformation and liquefaction of sand under cyclic stresses. *Soils Found* 15(1):29–44. <https://doi.org/10.3208/sandf1972.15.29>
- Ishihara K, Koga Y (1981) Case studies of liquefaction in the 1964 Niigata earthquake. *Soils Found* 21(3):35–52. https://doi.org/10.3208/sandf1972.21.3_35
- Varghese RM, Madhavi Latha G (2014) Shaking table tests to investigate the influence of various factors on the liquefaction resistance of sands. *Nat Hazards* 73:1337–1351. <https://doi.org/10.1007/s11069-014-1142-3>
- Yang KH, Thuo JN, Chen JW, Liu CN (2019) Failure investigation of a geosynthetic-reinforced soil slope subjected to rainfall. *Geosynth Int* 26(1):42–65. <https://doi.org/10.1680/jgein.18.00035>
- Nong ZZ, Park SS, Lee DE (2021) Comparison of sand liquefaction in cyclic triaxial and simple shear tests. *Soils Found* 61(4):1071–1085. <https://doi.org/10.1016/j.sandf.2021.05.002>
- Liu J, Chen G (2022) The correction factor of Monterey No. 0/30 sample with fines content liquefaction resistance between cyclic triaxial and cyclic hollow cylinder tests. *Sci Rep* 12(1):15927. <https://doi.org/10.1038/s41598-022-20002-3>
- Dyvik R, Berre T, Lacasse S, Raadim B (1987) Comparison of truly undrained and constant volume direct simple shear tests. *Geotechnique* 37(1):3–10. <https://doi.org/10.1680/geot.1987.37.1.3>
- Vaid YP, Sivathayalan S (1996) Static and cyclic liquefaction potential of Fraser Delta sand in simple shear and triaxial tests. *Can Geotech J* 33(2):281–289. <https://doi.org/10.1139/t96-007>
- Mao X, Fahey M (2003) Behaviour of calcareous soils in undrained cyclic simple shear. *Géotechnique* 53(8):715–727. <https://doi.org/10.1680/geot.2003.53.8.715>
- Papadopoulou A, Tika T (2008) The effect of fines on critical state and liquefaction resistance characteristics of non-plastic silty sands. *Soils Found* 48(5):713–725. <https://doi.org/10.3208/sandf.48.713>
- Zhang B, Muraleetharan KK, Liu C (2016) Liquefaction of unsaturated sands. *Int J Geomech* 16(6):D4015002. [https://doi.org/10.1061/\(ASCE\)GM.1943-5622.0000605](https://doi.org/10.1061/(ASCE)GM.1943-5622.0000605)
- Zhu Z, Zhang F, Peng Q, Dupla JC, Canou J, Cumunel G, Foerster E (2021) Assessment of the loading waveform on the cyclic liquefaction resistance with Hostun 31 sand. *Soil Dyn Earthq Eng* 150:106919. <https://doi.org/10.1016/j.soildyn.2021.106919>
- Latha GM, Lakkimsetti B (2022) Morphological perspectives to quantify and mitigate liquefaction in sands. *Indian Geotech J* 52(5):1244–1252. <https://doi.org/10.1007/s40098-022-00649-5>
- Ghadr S, Assadi-Langroudi A (2019) Effect of grain size and shape on undrained behaviour of sands. *Int J Geosynth Gr Eng* 5:18. <https://doi.org/10.1007/s40891-019-0170-1>
- Shahir H, Pak A, Ayoubi P (2016) A performance-based approach for design of ground densification to mitigate liquefaction. *Soil Dyn Earthq Eng* 90:381–394. <https://doi.org/10.1016/j.soildyn.2016.09.014>
- Nagula SS, Grabe J (2020) Coupled Eulerian Lagrangian based numerical modelling of vibro-compaction with model vibrator. *Comput Geotech* 123:103545. <https://doi.org/10.1016/j.compgeo.2020.103545>
- Duan W, Cai G, Liu S, Yuan J, Puppala AJ (2019) Assessment of ground improvement by vibro-compaction method for liquefiable deposits from in-situ testing data. *Int J Civ Eng* 17:723–735. <https://doi.org/10.1007/s40999-018-0348-2>
- Slocombe BC, Bell AL, Baez JI (2000) The densification of granular soils using vibro methods. *Geotechnique* 50(6):715–725. <https://doi.org/10.1680/geot.2000.50.6.715>
- Brennan AJ, Madabhushi SPG (2006) Liquefaction remediation by vertical drains with varying penetration depths. *Soil Dyn Earthq Eng* 26(5):469–475. <https://doi.org/10.1016/j.soildyn.2005.10.001>
- Howell R, Rathje EM, Kamai R, Boulanger R (2012) Centrifuge modeling of prefabricated vertical drains for liquefaction remediation. *J Geotech Geoenviron Eng* 138(3):262–271. [https://doi.org/10.1061/\(ASCE\)GT.1943-5606.0000604](https://doi.org/10.1061/(ASCE)GT.1943-5606.0000604)
- Howell R, Rathje EM, Boulanger R (2015) Evaluation of simulation models of lateral spread sites treated with prefabricated vertical drains. *J Geotech Geoenviron Eng* 141(1):04014076. [https://doi.org/10.1061/\(ASCE\)GT.1943-5606.0001185](https://doi.org/10.1061/(ASCE)GT.1943-5606.0001185)
- Chang WJ, Rathje EM, Stokoe KH, Cox BR (2004) Direct evaluation of effectiveness of prefabricated vertical drains in liquefiable sand. *Soil Dyn Earthq Eng* 24(9–10):723–731. <https://doi.org/10.1016/j.soildyn.2004.06.007>
- Kirkwood P, Dashti S (2019) Influence of prefabricated vertical drains on the seismic performance of similar neighbouring structures founded on liquefiable deposits. *Geotechnique* 69(11):971–985. <https://doi.org/10.1680/jgeot.17.P.077>
- Gallagher PM, Conlee CT, Rollins KM (2007) Full-scale field testing of colloidal silica grouting for mitigation of liquefaction risk. *J Geotech Geoenviron Eng* 133(2):186–196. [https://doi.org/10.1061/\(ASCE\)1090-0241\(2007\)133:2\(186\)](https://doi.org/10.1061/(ASCE)1090-0241(2007)133:2(186))
- Salvatore E, Modoni G, Mascolo MC, Grassi D, Spagnoli G (2020) Experimental evidence of the effectiveness and

- applicability of colloidal nanosilica grouting for liquefaction mitigation. *J Geotech Geoenviron Eng* 146(10):04020108. [https://doi.org/10.1061/\(ASCE\)GT.1943-5606.0002346](https://doi.org/10.1061/(ASCE)GT.1943-5606.0002346)
34. Rasouli H, Fatahi B, Nimbalkar S (2020) Liquefaction and post-liquefaction assessment of lightly cemented sands. *Can Geotech J* 57(2):173–188. <https://doi.org/10.1139/cgj-2018-0833>
 35. Sharma M, Satyam N (2021) Strength and durability of bio-cemented sands: Wetting-drying cycles, ageing effects, and liquefaction resistance. *Geoderma* 402:115359. <https://doi.org/10.1016/j.geoderma.2021.115359>
 36. Choi SG, Chang I, Lee M, Lee JH, Han JT, Kwon TH (2020) Review on geotechnical engineering properties of sands treated by microbially induced calcium carbonate precipitation (MICP) and biopolymers. *Constr Build Mater* 246:118415. <https://doi.org/10.1016/j.conbuildmat.2020.118415>
 37. Sopykhanova A, Maytanov A, Kiseleva A, Zhamiyeva R (2023) Problems of legal regulation and state policy measures related to nature management in the framework of achieving the SDGs: Examples from Russia and Kazakhstan. *Sustain* 15(2):1042. <https://doi.org/10.3390/su15021042>
 38. Koerner RM (2000) Emerging and future developments of selected geosynthetic applications. *J Geotech Geoenviron Eng* 126(4):293–306. [https://doi.org/10.1061/\(ASCE\)1090-0241\(2000\)126:4\(293\)](https://doi.org/10.1061/(ASCE)1090-0241(2000)126:4(293))
 39. Benessalah I, Arab A, Villard P, Merabet K, Bouferaa R (2016) Shear strength response of a geotextile-reinforced Chlef sand: a laboratory study. *Geotech Geol Eng* 34:1775–1790. <https://doi.org/10.1007/s10706-016-9988-7>
 40. Xu R, Fatahi B (2018) Influence of geotextile arrangement on seismic performance of mid-rise buildings subjected to MCE shaking. *Geotext Geomembr* 46(4):511–528. <https://doi.org/10.1016/j.geotextmem.2018.04.004>
 41. Altun S, Göktepe AB, Lav MA (2008) Liquefaction resistance of sand reinforced with geosynthetics. *Geosynth Int* 15(5):322–332. <https://doi.org/10.1680/gein.2008.15.5.322>
 42. Portelinha FH, Zornberg JG, Pimentel V (2014) Field performance of retaining walls reinforced with woven and nonwoven geotextiles. *Geosynth Int* 21(4):270–284. <https://doi.org/10.1680/gein.14.00014>
 43. Plácido R, Portelinha FHM, Futai MM (2018) Field and laboratory time-dependent behaviors of geotextiles in reinforced soil walls. *Geosynth Int* 25(2):215–229. <https://doi.org/10.1680/jgein.18.00003>
 44. Allen TM, Bathurst RJ (2019) Geosynthetic reinforcement stiffness characterization for MSE wall design. *Geosynth Int* 26(6):592–610. <https://doi.org/10.1680/jgein.19.00041>
 45. Kilic IE, Cengiz C, Edinçliler A, Guler E (2021) Seismic behavior of geosynthetic-reinforced retaining walls backfilled with cohesive soil. *Geotext Geomembr* 49(5):1256–1269. <https://doi.org/10.1016/j.geotextmem.2021.04.004>
 46. Lakkimsetti B, Gali ML (2023) Grain shape effects on the liquefaction response of geotextile-reinforced sands. *Int J Geosynth Gr Eng* 9:15. <https://doi.org/10.1007/s40891-023-00434-1>
 47. Latha GM, Murthy VS (2007) Effects of reinforcement form on the behavior of geosynthetic reinforced sand. *Geotext Geomembr* 25(1):23–32. <https://doi.org/10.1016/j.geotextmem.2006.09.002>
 48. Shao W, Cetin B, Li Y, Li J, Li L (2014) Experimental investigation of mechanical properties of sands reinforced with discrete randomly distributed fiber. *Geotech Geol Eng* 32:901–910. <https://doi.org/10.1007/s10706-014-9766-3>
 49. Kong Y, Zhou A, Shen F, Yao Y (2019) Stress–dilatancy relationship for fiber-reinforced sand and its modeling. *Acta Geotech* 14(6):1871–1881. <https://doi.org/10.1007/s11440-019-00834-6>
 50. Hamidi A, Hooresfand M (2013) Effect of fiber reinforcement on triaxial shear behavior of cement treated sand. *Geotext Geomembr* 36:1–9. <https://doi.org/10.1016/j.geotextmem.2012.10.005>
 51. Amini PF, Noorzad R (2018) Energy-based evaluation of liquefaction of fiber-reinforced sand using cyclic triaxial testing. *Soil Dyn Earthq Eng* 104:45–53. <https://doi.org/10.1016/j.soildyn.2017.09.026>
 52. Sivakumar Babu GL, Vasudevan AK, Haldar S (2008) Numerical simulation of fiber-reinforced sand behavior. *Geotext Geomembr* 26(2):181–188. <https://doi.org/10.1016/j.geotextmem.2007.06.004>
 53. Rajeswari JS, Sarkar R, Roy N, Bharti SD (2019) Bearing capacity of circular footing supported on coir fiber-reinforced soil. *Int J of Geotech Eng* 13(3):218–226. <https://doi.org/10.1080/19386362.2017.1334741>
 54. Sreya MV, Jayalekshmi BR, Venkataramana K (2022) Pore water pressure analysis in coir mat-reinforced soil incorporating soil-structure interaction. *Int J Geosynth Gr Eng* 8:11. <https://doi.org/10.1007/s40891-022-00354-6>
 55. Almeida MS, Hosseini I, Riccio M, Alexiew D (2015) Behavior of geotextile-encased granular columns supporting test embankment on soft deposit. *J Geotech Geoenviron Eng* 141(3):04014116. [https://doi.org/10.1061/\(ASCE\)GT.1943-5606.0001256](https://doi.org/10.1061/(ASCE)GT.1943-5606.0001256)
 56. Khabbazian M, Kaliakin VN, Meehan CL (2010) Numerical study of the effect of geosynthetic encasement on the behaviour of granular columns. *Geosynth Int* 17(3):132–143. <https://doi.org/10.1680/gein.2010.17.3.132>
 57. Murugesan S, Rajagopal K (2007) Model tests on geosynthetic-encased stone columns. *Geosynth Int* 14(6):346–354. <https://doi.org/10.1680/gein.2007.14.6.346>
 58. Mohapatra SR, Rajagopal K, Sharma J (2016) Direct shear tests on geosynthetic-encased granular columns. *Geotext Geomembr* 44(3):396–405. <https://doi.org/10.1016/j.geotextmem.2016.01.002>
 59. Dutta S, Nanda RP (2022) Waste rubber–soil mat for protection of structures from earthquake-induced liquefaction. *Int J Geosynth Gr Eng* 8:57. <https://doi.org/10.1007/s40891-022-00397-9>
 60. Horvath JS (1994) Expanded polystyrene (EPS) geofoam: an introduction to material behavior. *Geotext Geomembr* 13(4):263–280. [https://doi.org/10.1016/0266-1144\(94\)90048-5](https://doi.org/10.1016/0266-1144(94)90048-5)
 61. Witthoef AF, Kim H (2016) Numerical investigation of earth pressure reduction on buried pipes using EPS geofoam compressible inclusions. *Geosynth Int* 23(4):287–300. <https://doi.org/10.1680/jgein.15.00054>
 62. Zarnani S, Bathurst RJ (2007) Experimental investigation of EPS geofoam seismic buffers using shaking table tests. *Geosynth Int* 14(3):165–177. <https://doi.org/10.1680/gein.2007.14.3.165>
 63. Maheshwari BK, Singh HP, Saran S (2012) Effects of reinforcement on liquefaction resistance of Solani sand. *J Geotech Geoenviron Eng* 138(7):831–840. [https://doi.org/10.1061/\(ASCE\)GT.1943-5606.0000645](https://doi.org/10.1061/(ASCE)GT.1943-5606.0000645)
 64. Mousavi SA, Bastami M, Zahrai SM (2016) Large-scale seismic isolation through regulated liquefaction: a feasibility study. *Earthq Eng Vib* 15:579–595. <https://doi.org/10.1007/s11803-016-0350-0>
 65. Geng L, Tang L, Cong SY, Ling XZ, Lu J (2017) Three-dimensional analysis of geosynthetic-encased granular columns for liquefaction mitigation. *Geosynth Int* 24(1):45–59. <https://doi.org/10.1680/jgein.16.00014>
 66. Zhou L, Chen JF, Peng M, Zhu Y (2022) Liquefaction behavior of fiber-reinforced calcareous sands in unidirectional and multi-directional simple shear tests. *Geotext Geomembr* 50(4):794–806. <https://doi.org/10.1016/j.geotextmem.2022.04.003>
 67. ASTM Standard D6913 (2017) Standard test methods for particle-size distribution (gradation) of soils using sieve analysis.

- ASTM International, West Conshohocken, PA. <https://doi.org/10.1520/D6913-04R09E01>
68. Wadell H (1932) Volume, shape, and roundness of rock particles. *J Geol* 40(5):443–451. <https://doi.org/10.1086/623964>
 69. Wadell H (1935) Volume, shape, and roundness of quartz particles. *J Geol* 43(3):250–280. <https://doi.org/10.1086/624298>
 70. Lees G (1964) A new method for determining the angularity of particles. *Sedimentology* 3:2–21. <https://doi.org/10.1111/j.1365-3091.1964.tb00271.x>
 71. Krumbein WC, Sloss LL (1951) Stratigraphy and sedimentation. *Soil Sci* 71(5):401
 72. ASTM Standard D2487 (2020) Standard practice for classification of soils for engineering purposes (Unified Soil Classification System). ASTM International, West Conshohocken, PA. <https://doi.org/10.1520/D2487-17>
 73. ASTM Standard D854 (2016) Standard test methods for specific gravity of soil solids by water pycnometer. ASTM International, West Conshohocken, PA. <https://doi.org/10.1520/D0854-14>
 74. ASTM Standard D4253 (2019) Standard test methods for maximum index density and unit weight of soils using a vibratory table. ASTM International, West Conshohocken, PA. <https://doi.org/10.1520/D4253-16E01>
 75. ASTM Standard D4254 (2016) Standard test methods for minimum index density and unit weight of soils and calculation of relative density. ASTM International, West Conshohocken, PA. <https://doi.org/10.1520/D4254-16>
 76. Krishnaswamy NR, Isaac NT (1994) Liquefaction potential of reinforced sand. *Geotext Geomembr* 13(1):23–41. [https://doi.org/10.1016/0266-1144\(94\)90055-8](https://doi.org/10.1016/0266-1144(94)90055-8)
 77. Rasouli H, Fatahi B (2022) Liquefaction and post-liquefaction resistance of sand reinforced with recycled geofibre. *Geotext Geomembr* 50(1):69–81. <https://doi.org/10.1016/j.geotextmem.2021.09.002>
 78. Zhou L, Chen JF, Zhuang XY (2023) Undrained cyclic behaviors of fiber-reinforced calcareous sand under multidirectional simple shear stress path. *Acta Geotech*. <https://doi.org/10.1007/s11440-022-01780-6>
 79. Murugesan S, Rajagopal K (2010) Studies on the behavior of single and group of geosynthetic encased stone columns. *J Geotech Geoenvironmental Eng* 136(1):129–139. [https://doi.org/10.1061/\(ASCE\)GT.1943-5606.0000187](https://doi.org/10.1061/(ASCE)GT.1943-5606.0000187)
 80. Castro J (2017) Groups of encased stone columns: Influence of column length and arrangement. *Geotext Geomembranes* 45(2):68–80. <https://doi.org/10.1016/j.geotextmem.2016.12.001>
 81. Raitheil M, Kirchner A, Schade C, Leusink E (2005) Foundation of constructions on very soft soils with geotextile encased columns-state of the art. *Innov Grouting Soil Improv* 1–11. [https://doi.org/10.1061/40783\(162\)20](https://doi.org/10.1061/40783(162)20)
 82. Ou Yang F, Zhang JJ, Liao WM, Han JW, Tang YL, Bi JB (2017) Characteristics of the stress and deformation of geosynthetic-encased stone column composite ground based on large-scale model tests. *Geosynth Int* 24(3):242–254. <https://doi.org/10.1680/jgein.16.00028>
 83. Wang ZL, Li YC, Wang JG (2006) Numerical analysis of attenuation effect of EPS geofoam on stress-waves in civil defense engineering. *Geotext Geomembranes* 24(5):265–273. <https://doi.org/10.1016/j.geotextmem.2006.04.002>
 84. Athanasopoulos Zekkos A, Lamote K, Athanasopoulos GA (2012) Use of EPS geofoam compressible inclusions for reducing the earthquake effects on yielding earth retaining structures. *Soil Dyn Earthq Eng* 41:59–71. <https://doi.org/10.1016/j.soildyn.2012.05.004>
 85. Khan MI, Meguid MA (2021) A Numerical study on the role of EPS geofoam in reducing earth pressure on retaining structures under dynamic loading. *Int J Geosynth Gr Eng* 7(3):57. <https://doi.org/10.1007/s40891-021-00304-8>
 86. ASTM Standard D4595 (2017) Standard test method for tensile properties of geotextiles by the wide-width strip method. ASTM International, West Conshohocken, PA. <https://doi.org/10.1520/D4595-17>
 87. ASTM Standard D5261 (2018) Standard test method for measuring mass per unit area of geotextiles. ASTM International, West Conshohocken, PA. <https://doi.org/10.1520/D5261-10R18>
 88. ASTM Standard D5199 (2019) Standard test method for measuring the nominal thickness of geosynthetics. ASTM International, West Conshohocken, PA. <https://doi.org/10.1520/D5199-12R19>
 89. ASTM Standard D4751 (2021) Standard test methods for determining apparent opening size of a geotextile. ASTM International, West Conshohocken, PA. <https://doi.org/10.1520/D4751-21A>
 90. ASTM Standard D3822 (2020) Standard test method for tensile properties of single textile fibers. ASTM International, West Conshohocken, PA. <https://doi.org/10.1520/D3822-D3822M-14R20>
 91. ASTM Standard D1621 (2016) Standard test method for compressive properties of rigid cellular plastics. ASTM International, West Conshohocken, PA. <https://doi.org/10.1520/D1621-16>
 92. ASTM Standard D3999 (2012) Standard test methods for the determination of the modulus and damping properties of soils using the cyclic triaxial apparatus. ASTM International, West Conshohocken, PA. <https://doi.org/10.1520/D3999-11>
 93. Budhu M, Britto A (1987) Numerical analysis of soils in simple shear devices. *Soils Found* 27(2):31–41. https://doi.org/10.3208/sandf1972.27.2_31
 94. Budhu M (1988) Failure state of a sand in simple shear. *Can Geotech J* 25(2):395–400. <https://doi.org/10.1139/88-041>
 95. ASTM Standard D8296 (2019) Standard test method for consolidated undrained cyclic direct simple shear test under constant volume with load control or displacement control. ASTM International, West Conshohocken, PA. <https://doi.org/10.1520/D8296-19>
 96. Porcino D, Caridi G, Ghionna VN (2008) Undrained monotonic and cyclic simple shear behaviour of carbonate sand. *Geotechnique* 58(8):635–644. <https://doi.org/10.1680/geot.2007.00036>
 97. Gray DH, Al-Refeai T (1986) Behavior of fabric-versus fiber-reinforced sand. *J Geotech Eng* 112(8):804–820. [https://doi.org/10.1061/\(ASCE\)0733-9410\(1986\)112:8\(804\)](https://doi.org/10.1061/(ASCE)0733-9410(1986)112:8(804))
 98. Michalowski RL, Čermák J (2003) Triaxial compression of sand reinforced with fibers. *J Geotech geoenvironmental Eng* 129(2):125–136. [https://doi.org/10.1061/\(ASCE\)1090-0241\(2003\)129:2\(125\)](https://doi.org/10.1061/(ASCE)1090-0241(2003)129:2(125))
 99. Ibraim E, Diambra A, Wood DM, Russell AR (2010) Static liquefaction of fibre reinforced sand under monotonic loading. *Geotext Geomembranes* 28(4):374–385. <https://doi.org/10.1016/j.geotextmem.2009.12.001>
 100. Zhang X, Russell AR, Dong X (2022) Liquefaction responses of fibre reinforced sand in shaking table tests with a laminated shear stack. *Soil Dyn Earthq Eng* 162:107466. <https://doi.org/10.1016/j.soildyn.2022.107466>
 101. Zhang J, Yang Z, Yang Q, Yang G, Li G, Liu J (2021) Liquefaction behavior of fiber-reinforced sand based on cyclic triaxial tests. *Geosynth Int* 28(3):316–326. <https://doi.org/10.1680/jgein.20.00045>
 102. Festugato L, Fourie A, Consoli NC (2013) Cyclic shear response of fibre-reinforced cemented paste backfill. *Géotechnique Lett* 3(1):5–12. <https://doi.org/10.1680/geolett.12.00042>
 103. Consoli NC, Heineck KS, Casagrande MDT, Coop MR (2007) Shear strength behavior of fiber-reinforced sand considering triaxial tests under distinct stress paths. *J Geotech geoenvironmental Eng* 133(11):1466–1469. [https://doi.org/10.1061/\(ASCE\)1090-0241\(2007\)133:11\(1466\)](https://doi.org/10.1061/(ASCE)1090-0241(2007)133:11(1466))

104. Yang FO, Fan G, Wang K, Yang C, Lyu W, Zhang J (2021) A large-scale shaking table model test for acceleration and deformation response of geosynthetic encased stone column composite ground. *Geotext Geomembranes* 49(5):1407–1418. <https://doi.org/10.1016/j.geotextmem.2021.05.013>
105. Hubler JF, Athanasopoulos-Zekkos A, Zekkos D (2017) Monotonic, cyclic, and postcyclic simple shear response of three uniform gravels in constant volume conditions. *J Geotech Geoenviron Eng* 143(9):0001723. [https://doi.org/10.1061/\(ASCE\)GT.1943-5606.0001723](https://doi.org/10.1061/(ASCE)GT.1943-5606.0001723)
106. ElGhoraiby MA, Park H, Manzari MT (2020) Stress-strain behavior and liquefaction strength characteristics of Ottawa F65 sand. *Soil Dyn Earthq Eng* 138:106292. <https://doi.org/10.1016/j.soildyn.2020.106292>
107. Kokusho T, Kaneko Y (2018) Energy evaluation for liquefaction-induced strain of loose sands by harmonic and irregular loading tests. *Soil Dyn Earthq Eng* 114:362–377. <https://doi.org/10.1016/j.soildyn.2018.07.012>
108. Mele L, Tian JT, Lirer S, Flora A, Koseki J (2019) Liquefaction resistance of unsaturated sands: experimental evidence and theoretical interpretation. *Geotechnique* 69(6):541–553. <https://doi.org/10.1680/jgeot.18.P.042>
109. Zhu Z, Zhang F, Peng Q, Dupla JC, Canou J, Cumunel G, Foerster E (2021) Effect of the loading frequency on the sand liquefaction behaviour in cyclic triaxial tests. *Soil Dyn Earthq Eng* 147:106779. <https://doi.org/10.1016/j.soildyn.2021.106779>
110. Amini F, Sama KM (1999) Behavior of stratified sand–silt–gravel composites under seismic liquefaction conditions. *Soil Dyn Earthq Eng* 18(6):445–455. [https://doi.org/10.1016/S0267-7261\(99\)00011-1](https://doi.org/10.1016/S0267-7261(99)00011-1)
111. Saxena SK, Reddy KR, Avramidis AS (1988) Liquefaction resistance of artificially cemented sand. *J Geotech Eng* 114(12):1395–1413. [https://doi.org/10.1061/\(ASCE\)0733-9410\(1988\)114:12\(1395\)](https://doi.org/10.1061/(ASCE)0733-9410(1988)114:12(1395))
112. Idriss IM, Dobry R, Singh RD (1978) Nonlinear behavior of soft clays during cyclic loading. *J Geotech Eng Div* 104(12):1427–1447. <https://doi.org/10.1061/AJGEB6.0000727>
113. Yang ZX, Li XS, Yang J (2007) Undrained anisotropy and rotational shear in granular soil. *Geotechnique* 57(4):371–384. <https://doi.org/10.1680/geot.2007.57.4.371>
114. Kantesaria N, Sachan A (2021) Cyclic degradation and pore-water pressure response of high-plasticity compacted clay. *J Geotech Geoenviron Eng* 147(11):04021113. [https://doi.org/10.1061/\(ASCE\)GT.1943-5606.0002630](https://doi.org/10.1061/(ASCE)GT.1943-5606.0002630)
115. Figueroa JL, Saada AS, Liang L, Dahisaria NM (1994) Evaluation of soil liquefaction by energy principles. *J Geotech Eng* 120(9):1554–1569. [https://doi.org/10.1061/\(ASCE\)0733-9410\(1994\)120:9\(1554\)](https://doi.org/10.1061/(ASCE)0733-9410(1994)120:9(1554))
116. Polito CP, Green RA, Lee J (2008) Pore pressure generation models for sands and silty soils subjected to cyclic loading. *J Geotech Geoenviron Eng* 134(10):1490–1500. [https://doi.org/10.1061/\(ASCE\)1090-0241\(2008\)134:10\(1490\)](https://doi.org/10.1061/(ASCE)1090-0241(2008)134:10(1490))
117. Kokusho T (2013) Liquefaction potential evaluations: Energy-based method versus stress-based method. *Can Geotech J* 50(10):1088–1099. <https://doi.org/10.1139/cgj-2012-0456>
118. Kokusho T (2021) Energy-based liquefaction evaluation for induced strain and surface settlement—evaluation steps and case studies. *Soil Dyn Earthq Eng* 143:106552. <https://doi.org/10.1016/j.soildyn.2020.106552>
119. Polito C, Green RA, Dillon E, Sohn C (2013) Effect of load shape on relationship between dissipated energy and residual excess pore pressure generation in cyclic triaxial tests. *Can Geotech J* 50(11):1118–1128. <https://doi.org/10.1139/cgj-2012-0379>
120. Jain A, Mittal S, Shukla SK (2023) Energy-based approach to study liquefaction triggering in homogeneous and stratified soils under consolidated undrained cyclic loading. *Eng Geol.* <https://doi.org/10.1016/j.enggeo.2023.107151>
121. Yang ZX, Pan K (2018) Energy-based approach to quantify cyclic resistance and pore pressure generation in anisotropically consolidated sand. *J Mater Civ Eng* 30(9):4018203. [https://doi.org/10.1061/\(ASCE\)MT.1943-5533.0002419](https://doi.org/10.1061/(ASCE)MT.1943-5533.0002419)
122. Tabora DMG, Potts DM, Zdravković L (2016) On the assessment of energy dissipated through hysteresis in finite element analysis. *Comput Geotech* 71:180–194. <https://doi.org/10.1016/j.compgeo.2015.09.001>
123. Jin H, Guo L, Sun H, Wu T, Shi L, Cai Y (2022) Energy-based evaluation of undrained cyclic behavior of marine soft clay under multidirectional simple shear stress paths. *Acta Geotech.* <https://doi.org/10.1007/s11440-022-01765-5>
124. Zavala GJ, Pando MA, Park Y, Aguilar R (2022) Specific dissipated energy as a failure predictor for uniform sands under constant volume cyclic simple shear loading. *KSCE J Civ Eng* 26(2):703–714. <https://doi.org/10.1007/s12205-021-1205-4>
125. Moayed RZ, Alibolandi M (2018) Effect of geotextile reinforcement on cyclic undrained behavior of sand. *Soil Dyn Earthq Eng* 104:395–402. <https://doi.org/10.1016/j.soildyn.2017.11.013>
126. Su L, Zhou L, Zhang X, Ling X (2022) Experimental and numerical modeling on liquefaction resistance of geotextile reinforced sand. *Soil Dyn Earthq Eng* 159:107345. <https://doi.org/10.1016/j.soildyn.2022.107345>
127. Noorzad R, Fardad Amini P (2014) Liquefaction resistance of Babolsar sand reinforced with randomly distributed fibers under cyclic loading. *Soil Dyn Earthq Eng* 66:281–292. <https://doi.org/10.1016/j.soildyn.2014.07.011>
128. Chegenizadeh A, Keramatikerman M, Nikraz H (2018) Liquefaction resistance of fibre reinforced low-plasticity silt. *Soil Dyn Earthq Eng* 104:372–377. <https://doi.org/10.1016/j.soildyn.2017.11.004>
129. Ghadr S, Samadzadeh A, Bahadori H, Assadi-Langroudi A (2020) Liquefaction resistance of fibre-reinforced silty sands under cyclic loading. *Geotext Geomembranes* 48(6):812–827. <https://doi.org/10.1016/j.geotextmem.2020.07.002>
130. Tang L, Cong S, Ling X, Lu J, Elgamal A (2015) Numerical study on ground improvement for liquefaction mitigation using stone columns encased with geosynthetics. *Geotext Geomembranes* 43(2):190–195. <https://doi.org/10.1016/j.geotextmem.2014.11.011>
131. Rashma RSV, Jayalekshmi BR, Shivashankar R (2022) Liquefaction mitigation potential of improved ground using pervious concrete columns. *Indian Geotech J* 52(1):205–226. <https://doi.org/10.1007/s40098-021-00536-5>
132. Bahadori H, Farzalizadeh R, Barghi A, Hasheminezhad A (2018) A comparative study between gravel and rubber drainage columns for mitigation of liquefaction hazards. *J Rock Mech Geotech Eng* 10(5):924–934. <https://doi.org/10.1016/j.jrmge.2018.03.008>

Publisher's Note Springer Nature remains neutral with regard to jurisdictional claims in published maps and institutional affiliations.

Springer Nature or its licensor (e.g. a society or other partner) holds exclusive rights to this article under a publishing agreement with the author(s) or other rightsholder(s); author self-archiving of the accepted manuscript version of this article is solely governed by the terms of such publishing agreement and applicable law.